SUPPORTING INFORMATION

Structure, Location and Spatial Proximities of Hydroxyls on γ–Alumina Crystallites by High-Resolution Solid-State NMR and DFT Modelling: Why Edges hold the Key

Ana T. F. Batista [a,$], Thomas Pigeon [a,$], Jordan Meyet [a], Dorothea Wisser [a,b,+], Mickael Rivallan[a], David Gajan[b], Leonor Catita[a], Fabrice Diehl[a], Anne-Sophie Gay [a], Céline Chizallet [a], Anne Lesage [b,*], and Pascal Raybaud [a,c,*]

[a] IFP Energies nouvelles, Rond-point de l'échangeur de Solaize, 69360 Solaize (France)

[b] Université de Lyon, CNRS, ENS Lyon, Université Lyon 1, Centre de RMN à hauts champs de Lyon, UMR 5082, 5 rue de la Doua, 69100 Villeurbanne (France)

[c] ENS Lyon, CNRS, Laboratoire de Chimie UMR 5182, 46 Allée d'Italie, 69364 Lyon (France)

[$] A.T.F.B and TP contributed equally to this paper.

+ current address: Erlangen Center for Interface Research and Catalysis, Friedrich-Alexander-Universität Erlangen-Nürnberg, Egerlandstrasse 3, 91058 Erlangen (Germany)

Corresponding authors: pascal.raybaud@ifpen.fr and anne.lesage@ens-lyon.fr

SI 1. Alumina sample characterization

X-ray diffraction was performed on a PANalytical X'Pert Pro diffractometer with a copper anode (Kα=0.15402 nm) and a X'célérator detector, scanning an angle range of 5 to 72° 2θ (Figure S1).

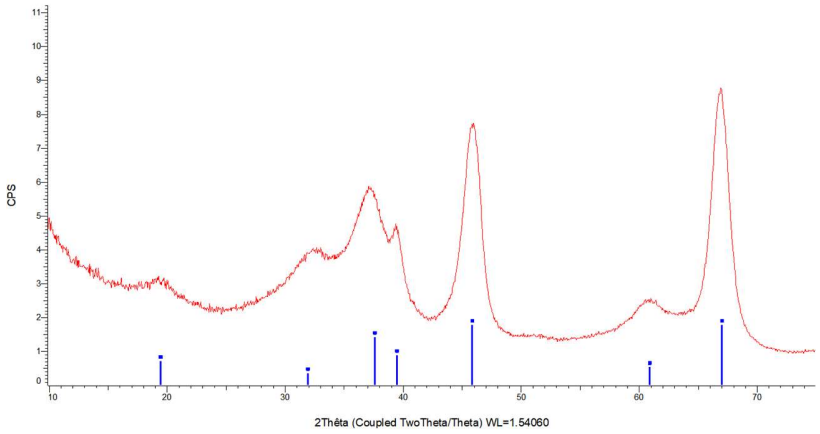

Figure S1. XRD diffractograms of the γ–alumina sample (blue-γ-Al_2O_3 reference ICDD n° 00-010-0425).

N_2 physisorption was done using a Micromeritics ASAP 2420 equipment, samples were pre-treated at 350°C for 3h under vacuum. Hg porosimetry was done using a Micromeritics Autopore IV equipment, samples were pre-treated at 250°C for 3h. The BET surface is 183±9 $m^2\ g^{-1}$, the mesoporous volume 0.49±0.02 mL g^{-1} and the mesopore diameter evaluated at half the mesoporous volume is 9.8±0.2 nm.

High resolution Transmission Electron Microscopy (HR-TEM) images in Bright field mode and nanobeam electron diffraction patterns were acquired on a JEOL JEM 2100F microscope (Figure S2). The following crystallite dimensions (from about 30 measurements) were measured: length between 4 and 16 nm (average 12.5 nm), width between 4 and 11 nm (average 6 nm) and thickness approximately between 4 and 6 nm.

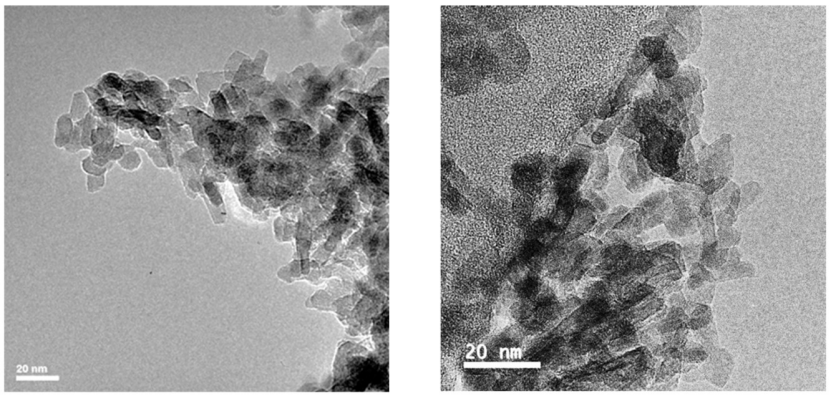

Figure S2. TEM images of γ–alumina (scale: 20 nm). Reprinted from ref.1, Copyright 2019, with permission from Elsevier.

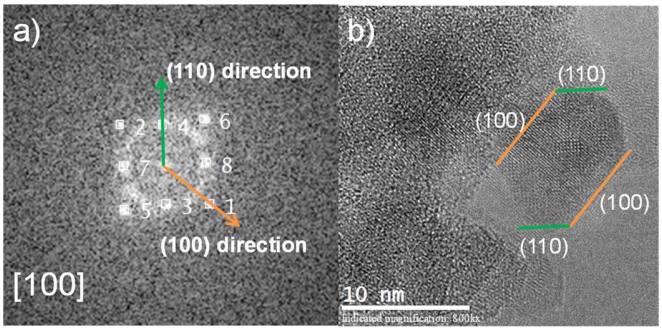

Figure S3. Plane indexation of the illustrated crystallites (b) performed by (a) Fourier transform indexation from a HR-TEM image. Reprinted from ref.1, Copyright 2019, with permission from Elsevier.

SI 2. Complementary DFT information

Following a similar approach as for the construction of the (100)/$(110)_l$-A1investigated in ref.1, $(110)_b$/$(110)_l$ nano-rod models (for the A1 and L1 type of $(110)_l$) were built from the alumina slab models obtained in ref.2, themselves obtained by the simulation of the dehydration of boehmite slabs. The $(110)_b$/(100) rod models were built by using an approach based on the transformation of a (010)/(100) nano-rod of boehmite.

Given the low symmetry of the bulk, there are two types of edges on each 'nano-rod' model as illustrated in **Figures S4** and **S5**. In **Figure S5**, the thicknesses of the vacuum between each periodic replica (from 22 Å for (100) facet to 27 Å for $(110)_l$ facets) were chosen so that the total energy is converged with a tolerance variation of 10^{-2} eV. The rod thicknesses in the two directions perpendicular to the main rod axis, was chosen so that the edge adsorption energy was constant (5 $kJ.mol^{-1}$ precision) with respect to the variation of the rod dimensions. This is the best compromise according to the CPU simulation time and the number of explored configurations.

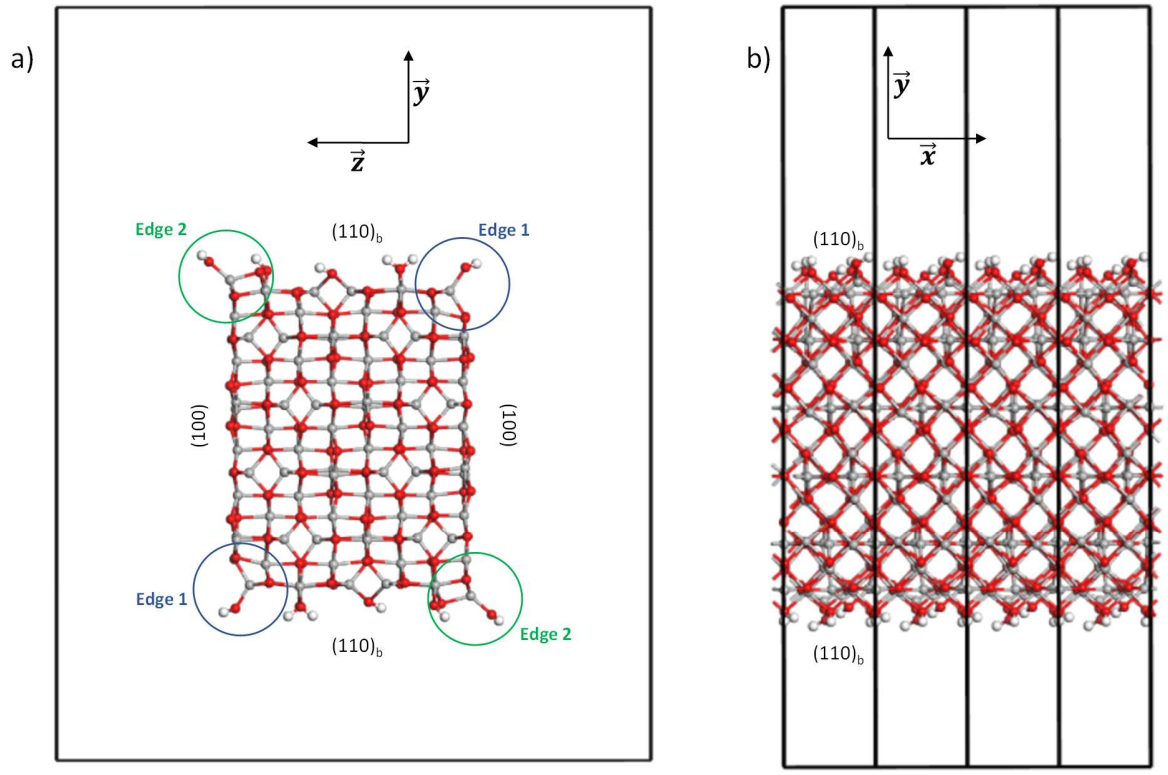

Figure S4: Front view (a) and side view with 4 duplicated cells (b) of a $(110)_b$/(100) nano-rod periodic model. Color coding: red balls: O atoms; white balls: H atoms; gray balls: Al atoms.

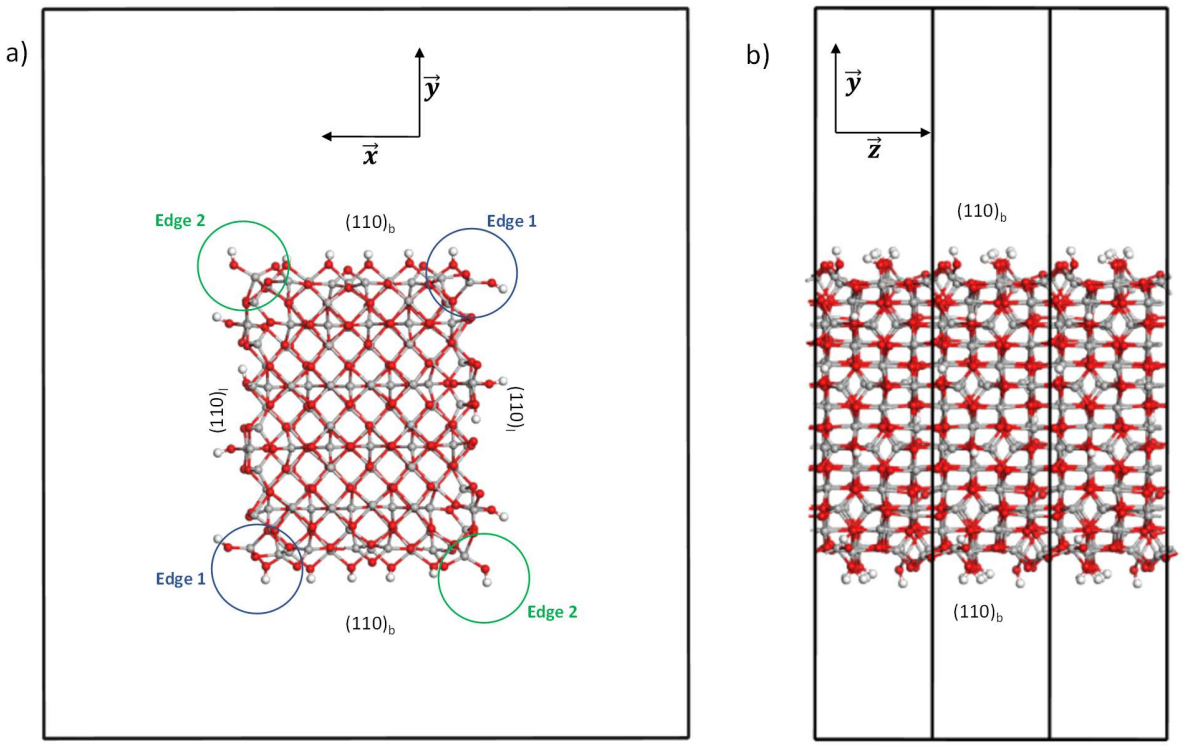

Figure S5: Front view (a) and side view with 3 duplicated cells (b) of a $(110)_b/(110)_l$-L1 nano-rod periodic model. Color coding: red balls, O atoms; white balls, H atoms; gray balls: Al atoms.

$(110)_b/(100)$ edge	$Al_{80}O_{126}H_{12}$
Periodic cell dimensions (Å)	a = 5.531 b = 45.860 c = 36.124

Table S1: Cell parameters of the nano-rod model presented in **Figure S4**.

$(110)_b/(110)_l$-L1 edge	$Al_{120}O_{208}H_{56}$
Periodic cell dimensions (Å)	a = 44.244 b = 50.028 c = 8.028

Table S2: Cell parameters of the nano-rod model presented in **Figure S5**.

SI 3. Structural models of the γ–alumina facets and edges before and after chlorination

Facet	$(110)_b$	$(110)_l$				(111)		
		A1	A2	L1	L2	D1	D2	D2*
Figures	S6	S7	S8	S9	S10	S11	S12	S13
Edge	(100)/$(110)_l$-A1		$(110)_b$/(100)		$(110)_b$/$(110)_l$-A1		$(110)_b$/$(110)_l$-L1	
Figures	S14	S15*	S16		S17	S18*	S19	S20*

Table S3. List of facets and edges used for the simulation of chlorination and corresponding labels of figures used in **SI 3**. All structures are those obtained at T=700 K and at T=800 K (*).

A) Facets

Facet	700 K and 10^{-4} bar	800 K and 10^{-6} bar
(111)-D1	9.8	9.8
(111)-D2	9.8	7.3
(111)-P1_2	9.8	7.3
$(110)_l$-L1	12.0	3.0
$(110)_l$-L2	12.0	3.0
$(110)_l$-A1	9.0	3.0
$(110)_l$-A2	9.0	3.0
$(110)_b$	9.0	4.5

Table S4. Hydration states ($OH.nm^{-2}$) of the facets according to the interval of experimental (T, P) conditions considered.

If one except the (111)_D2 facet (* in **Table S4**), all other facets do not contain any exchangeable μ_1-OH species at 800 K and 10^{-6} bar. So, in what follows, only facets containing exchangeable μ_1-OH species are reported.

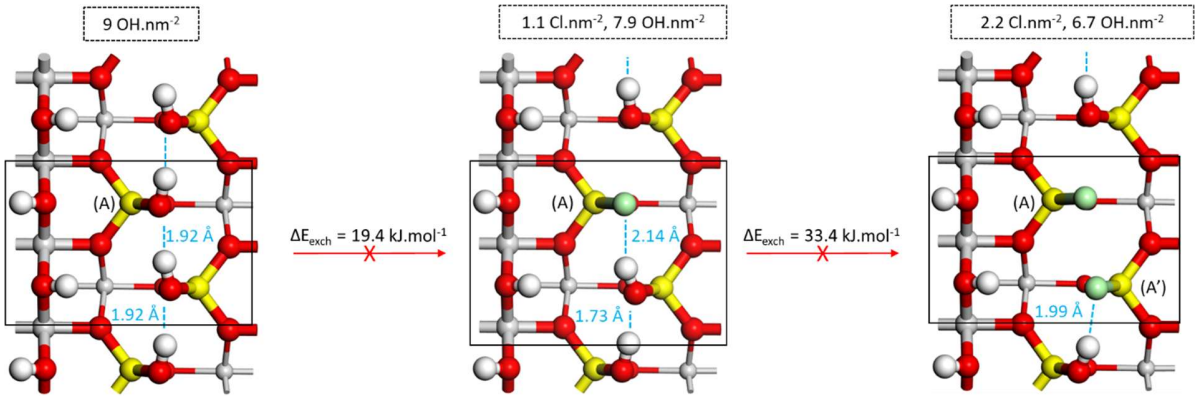

Figure S6. Top views of $(110)_b$ facet models hydrated at 700 K, before and after chlorination. Color coding: red-oxygen; grey-aluminum; yellow-aluminum connected to μ_1-OH which can be substituted by Cl; white-hydrogen; green-chlorine. Blue dashed lines indicate hydrogen-bonds (bond length's threshold of 2.5 Å) with noticeable hydrogen-bonds distances. Al sites of μ_1-OH are identified by letters according to the notation in **Table S5**. The Cl/OH coverages of the facet are reported in the rectangular dotted frames.

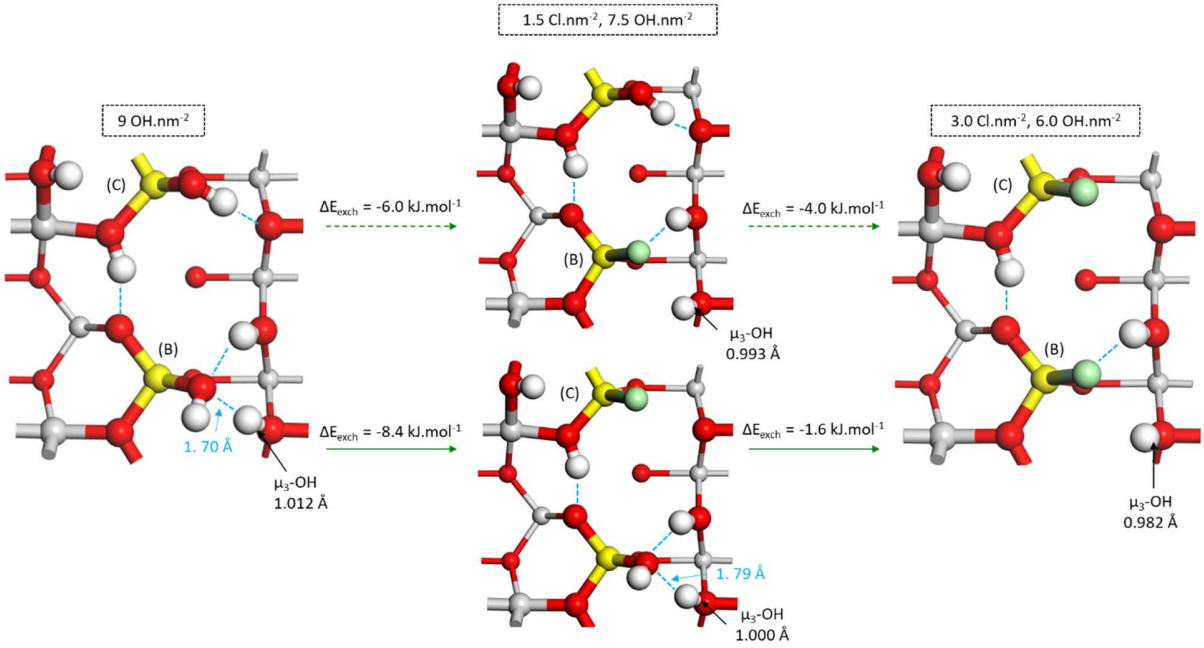

Figure S7. Top views of $(110)_l$-A1 facet models hydrated at 700 K, before and after chlorination. Color coding: red-oxygen; grey-aluminum; yellow-aluminum connected to μ_1-OH which can be substituted by Cl; white-hydrogen; green-chlorine. Blue dashed lines indicate hydrogen-bonds (bond length's threshold of 2.5 Å) with noticeable hydrogen-bonds distances. Al sites of μ_1-OH are identified by letters according to the notation in **Table S5**. The Cl/OH coverages of the facet are reported in the rectangular dotted frames.

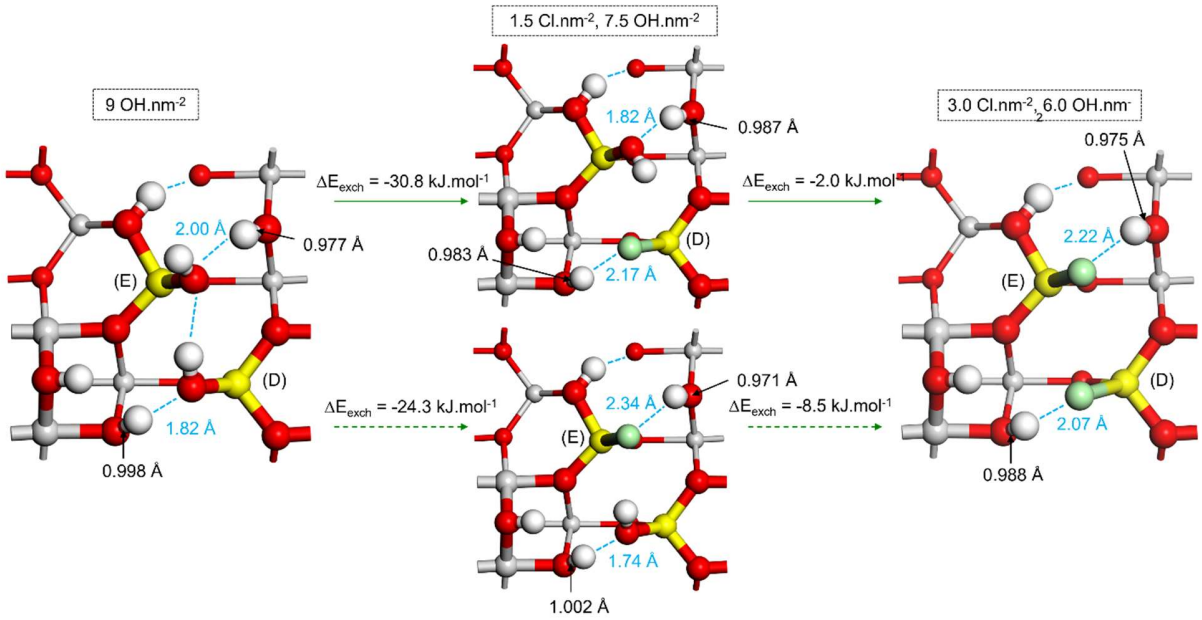

Figure S8. Top views of $(110)_l$-A2 facet models hydrated at 700 K, before and after chlorination. Color coding: red-oxygen; grey-aluminum; yellow-aluminum connected to μ_1-OH which can be substituted by Cl; white-hydrogen; green-chlorine. Blue dashed lines indicate hydrogen-bonds (bond length's threshold of 2.5 Å) with noticeable hydrogen-bonds distances. Al sites of μ_1-OH are identified by letters according to the notation in **Table S5**. The Cl/OH coverages of the facet are reported in the rectangular dotted frames.

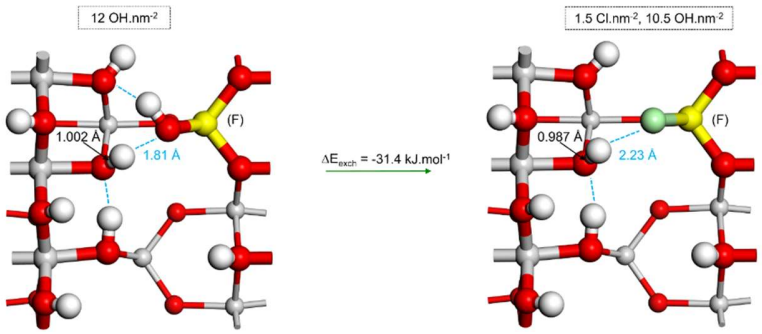

Figure S9. Top views of $(110)_l$-L1 facet models hydrated at 700 K, before and after chlorination. Color coding: red-oxygen; grey-aluminum; yellow-aluminum connected to μ_1-OH which can be substituted by Cl; white-hydrogen; green-chlorine. Blue dashed lines indicate hydrogen-bonds (bond length's threshold of 2.5 Å) with noticeable hydrogen-bonds distances. Al sites of μ_1-OH are identified by letters according to the notation in **Table S5**. The Cl/OH coverages of the facet are reported in the rectangular dotted frames.

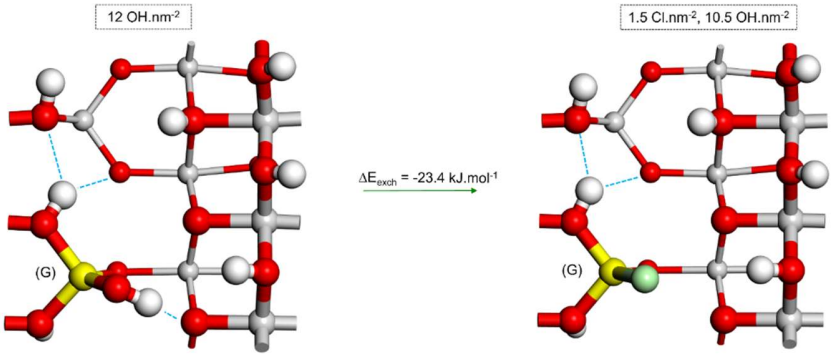

Figure S10. Top views of $(110)_I$-L2 facet models hydrated at 700 K, before and after chlorination. Color coding: red-oxygen; grey-aluminum; yellow-aluminum connected to μ_1-OH which can be substituted by Cl; white-hydrogen; green-chlorine. Blue dashed lines indicate hydrogen-bonds (bond length's threshold of 2.5 Å) with noticeable hydrogen-bonds distances. Al sites of μ_1-OH are identified by letters according to the notation in **Table S5**. The Cl/OH coverages of the facet are reported in the rectangular dotted frames.

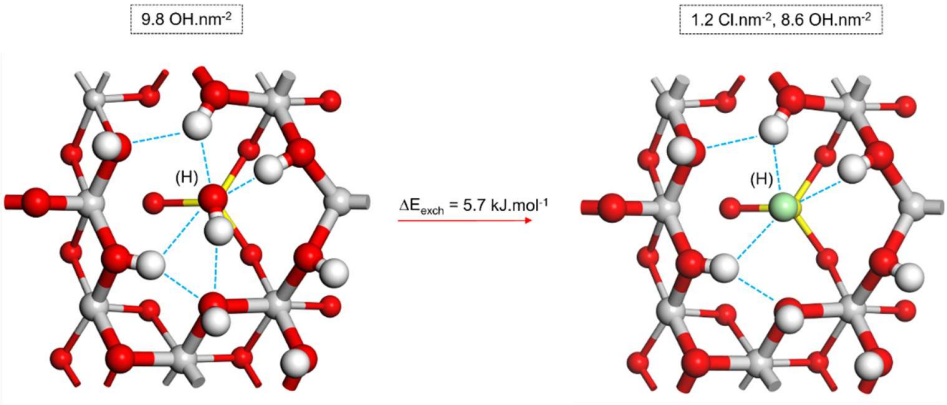

Figure S11. Top views of (111)-D1 facet models hydrated at 700 K, before and after chlorination. Color coding: red-oxygen; grey-aluminum; yellow-aluminum connected to μ_1-OH which can be substituted by Cl; white-hydrogen; green-chlorine. Blue dashed lines indicate hydrogen-bonds (bond length's threshold of 2.5 Å) with noticeable hydrogen-bonds distances. Al sites of μ_1-OH are identified by letters according to the notation in **Table S5**. The Cl/OH coverages of the facet are reported in the rectangular dotted frames.

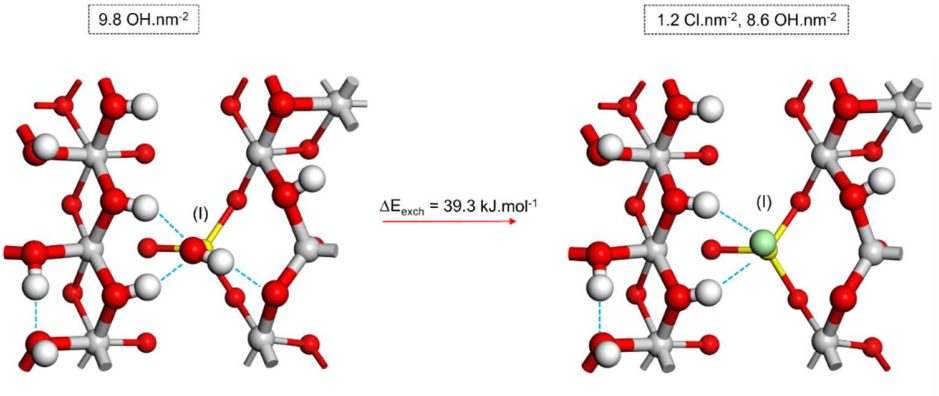

Figure S12. Top views of (111)-D2 facet models hydrated at 700 K, before and after chlorination. Color coding: red-oxygen; grey-aluminum; yellow-aluminum connected to μ_1-OH which can be substituted by Cl; white-hydrogen; green-chlorine. Blue dashed lines indicate hydrogen-bonds (bond length's threshold of 2.5 Å) with noticeable hydrogen-bonds distances. Al sites of μ_1-OH are identified by letters according to the notation in **Table S5.** The Cl/OH coverages of the facet are reported in the rectangular dotted frames.

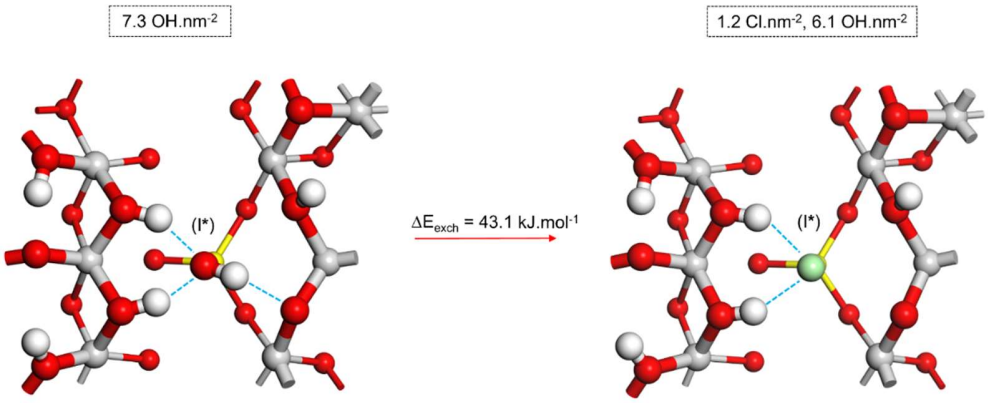

Figure S13. Top views of (111)-D2 facet models hydrated at 800 K, before and after chlorination. Color coding: red-oxygen; grey-aluminum; yellow-aluminum connected to μ_1-OH which can be substituted by Cl; white-hydrogen; green-chlorine. Blue dashed lines indicate hydrogen-bonds (bond length's threshold of 2.5 Å) with noticeable hydrogen-bonds distances. Al sites of μ_1-OH are identified by letters according to the notation in **Table S5**. The Cl/OH coverages of the facet are reported in the rectangular dotted frames.

B) Edges

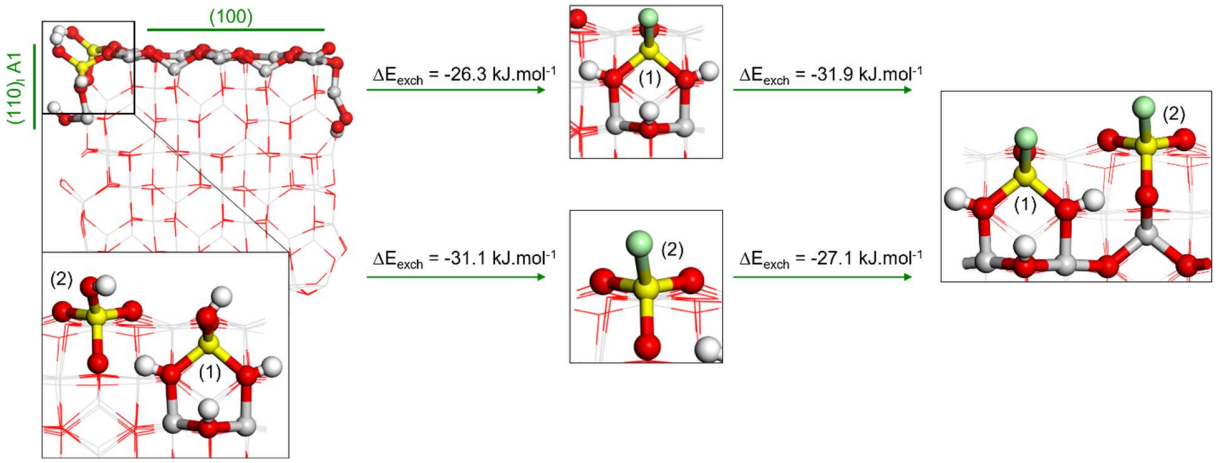

Figure S14. (100)/(110)$_l$-A1 hydrated models at 700 K, before and after chlorination. Color coding: red-oxygen; grey-aluminum; yellow-aluminum connected to μ_1-OH which can be substituted by Cl; white-hydrogen; green-chlorine. μ_1-OH are identified by numbers according to the notation in **Table S5**.

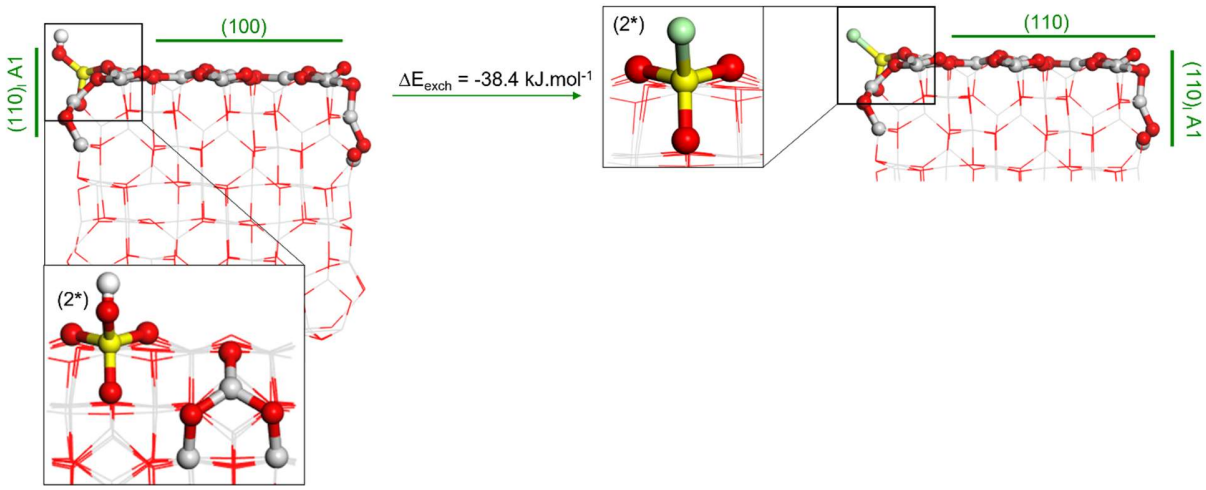

Figure S15. (100)/(110)$_l$-A1 hydrated models at 800 K, before and after chlorination. Color coding: red-oxygen; grey-aluminum; yellow-aluminum connected to μ_1-OH which can be substituted by Cl; white-hydrogen; green-chlorine. μ_1-OH are identified by numbers according to the notation in **Table S5**.

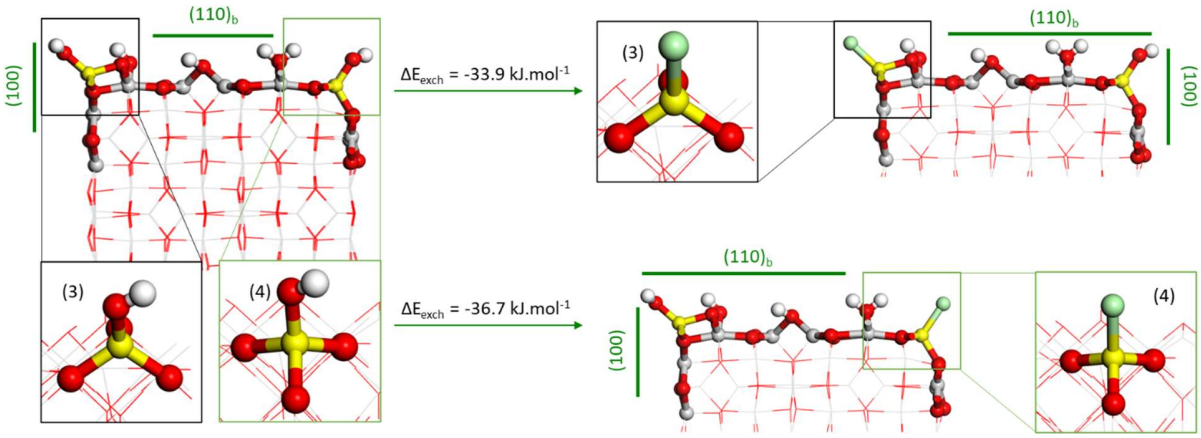

Figure S16. $(110)_b/(100)$ hydrated models at 700 K, before and after chlorination. Color coding: red-oxygen; grey-aluminum; yellow-aluminum connected to μ_1-OH which can be substituted by Cl; white-hydrogen; green-chlorine. μ_1-OH are identified by numbers according to the notation in **Table S5**.

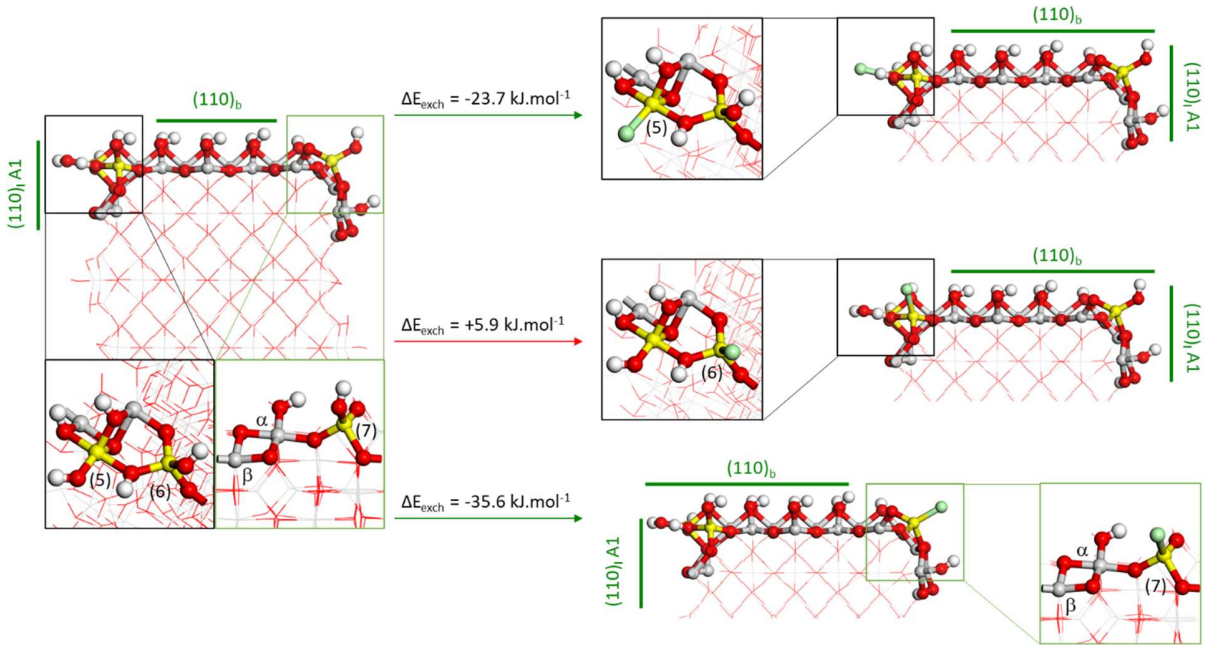

Figure S17. $(110)_b/(110)_l$-A1 hydrated models at 700 K, before and after chlorination. Color coding: red-oxygen; grey-aluminum; yellow-aluminum connected to μ_1-OH which can be substituted by Cl; white-hydrogen; green-chlorine. μ_1-OH are identified by numbers according to the notation in **Table S5**.

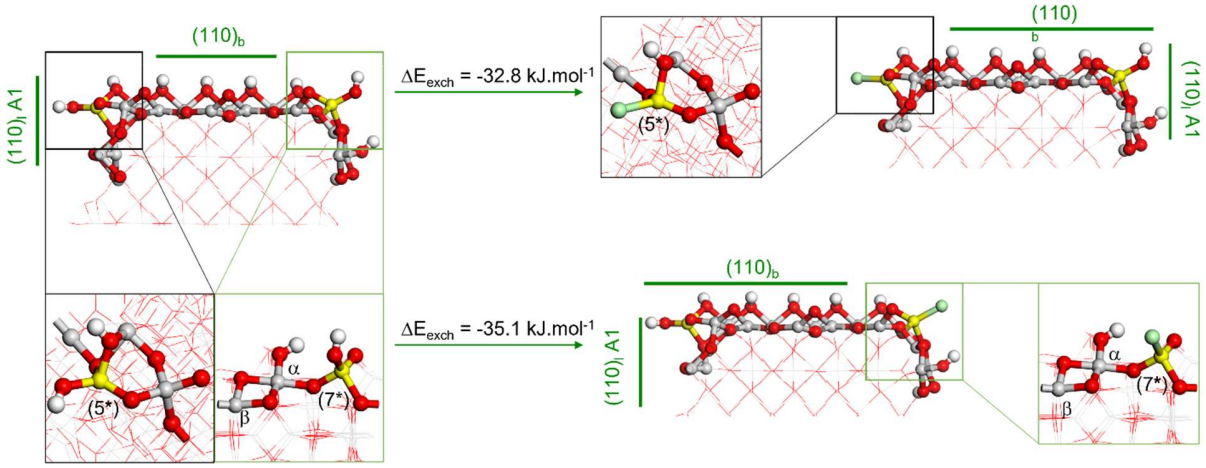

Figure S18. $(110)_b/(110)_l$-A1 hydrated models at 800 K, before and after chlorination. Color coding: red-oxygen; grey-aluminum; yellow-aluminum connected to μ_1-OH which can be substituted by Cl; white-hydrogen; green-chlorine. μ1-OH are identified by numbers according to the notation in **Table S5**.

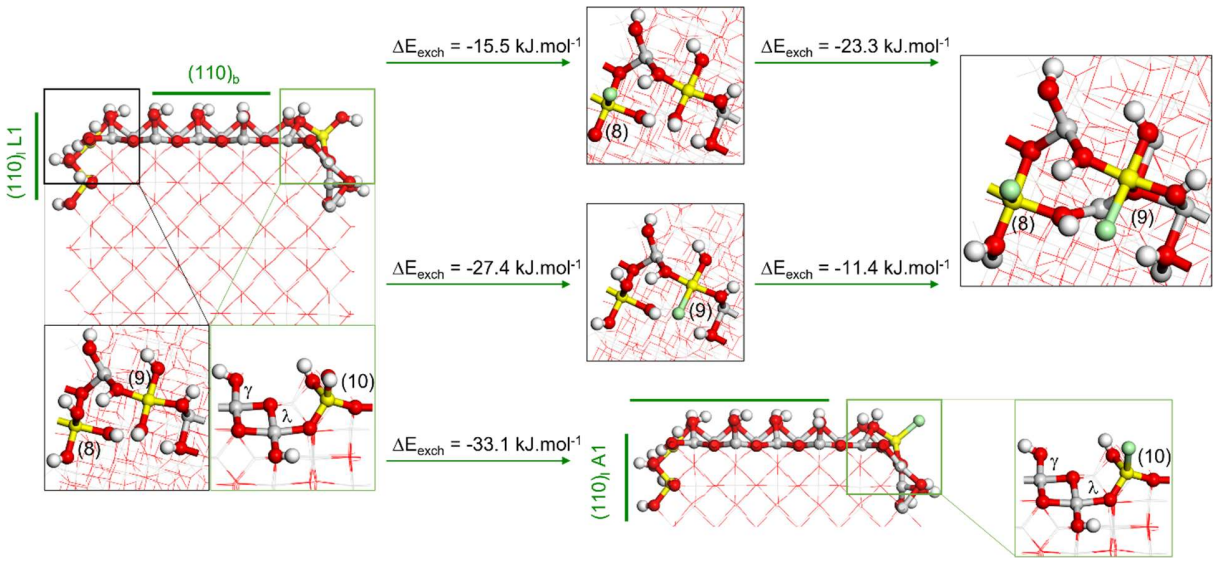

Figure S19. $(110)_b$/$(110)_l$-L1 hydrated models at 700 K, before and after chlorination. Color coding: red-oxygen; grey-aluminum; yellow-aluminum connected to μ_1-OH which can be substituted by Cl; white-hydrogen; green-chlorine. μ_1-OH are identified by numbers according to the notation in **Table S5**.

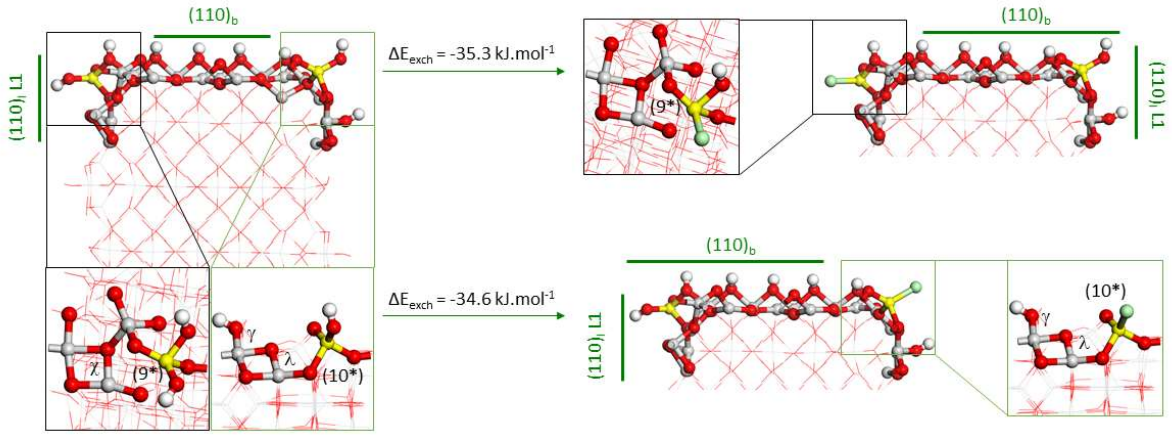

Figure S20. $(110)_b$/$(110)_l$-L1 hydrated models at 800 K, before and after chlorination. Color coding: red-oxygen; grey-aluminum; yellow-aluminum connected to μ_1-OH which can be substituted by Cl; white-hydrogen; green-chlorine. μ_1-OH are identified by numbers according to the notation in **Table S5**.

SI 4. Nature of OH sites and energetics of the chlorination on facets and edges

For the chlorination process, the stable facets and edges dehydroxylated at 700 or 800 K (10^{-4} and 10^{-6} bar respectively) were considered to mimic the experimental conditions. Starting from the hydrated structure, chlorination of the facet/edge occurs by adding gas phase hydrogen chloride (HCl), leading to the substitution of surface hydroxyl group and release of water (H_2O) from the facet/edge according to the following equation:

$$Al_n - OH + HCl_{gas} \rightleftarrows Al_n - Cl + H_2O_{gas} \qquad (1)$$

where n is the coordination of the Al ion bearing the substituted OH group. The energy of Cl exchange with the surface (ΔE_{exch}) is calculated according to:

$$\Delta E_{exch} = E(Al_n - Cl) + E(H_2O) - E(Al_n - OH) - E(HCl) \qquad (2)$$

	Facet or Edge	ID	Site	H-bond type	ΔE_{exch} (kJ.mol^{-1}) (0 K)
Facet	$(110)_b$	**A**	$Al_{IV\text{-}Td}$	donor/acceptor	**19.4**
	$(110)_l$-A1	**B**	$Al_{IV\text{-}Td}$	donor/acceptor	**-6.0**
		C	$Al_{IV\text{-}Td}$	donor	**-8.4**
		BC	$Al_{IV\text{-}Td}$	donor/acceptor	**-5.0**
	$(110)_l$-A2	**D**	$Al_{IV\text{-}Td}$	donor/acceptor	**-30.8**
		E	$Al_{IV\text{-}Td}$	acceptor	**-24.3**
		DE	$Al_{IV\text{-}Td}$	donor/acceptor	**-16.4**
	$(110)_l$-L1	**F**	$Al_{IV\text{-}Td}$	donor/acceptor	**-31.4**
	$(110)_l$-L2	**G**	$Al_{IV\text{-}Td}$	donor	**-23.4**
	(111)-D1	**H**	$Al_{IV\text{-}Td}$	donor/acceptor	**5.7**
	(111)-D2	**I**	$Al_{IV\text{-}Td}$	donor/acceptor	**39.3**
		I*	$Al_{IV\text{-}Td}$	donor/acceptor	**43.1**
edges	(100)/$(110)_l$-A1	**1**	$Al_{IV\text{-}Td}$	free	**-26.3**
		2	$Al_{IV\text{-}Td}$	free	**-31.1**
		12	$Al_{IV\text{-}Td}$	free	**-29.1**
		2*	$Al_{IV\text{-}Td}$	free	**-38.4**
	$(110)_b$/(100)	**3**	$Al_{IV\text{-}Td}$	free	**-33.9**
		4	$Al_{IV\text{-}Td}$	free	**-36.7**
	$(110)_b$/$(110)_l$-A1	**5**	$Al_{V\text{-}Oh}$	free	**-23.7**
		6	$Al_{IV\text{-}Td}$	donor/acceptor	**5.9**
		7	$Al_{IV\text{-}Td}$	free	**-35.6**
		5*	$Al_{IV\text{-}Td}$	free	**-32.8**
		7*	$Al_{IV\text{-}Td}$	free	**-35.1**
	$(110)_b$/$(110)_l$-L1	**8**	$Al_{VI\text{-}Oh}$	free	**-15.5**
		9	$Al_{V\text{-}Oh}$	acceptor	**-27.4**
		10	$AlI_{V\text{-}Td}$	donor/acceptor	**-33.1**
		8/9	$Al_{VI\ /\ V\text{-}Oh}$	free / acceptor	**-19.4**
		9*	$Al_{IV\text{-}Td}$	free	**-35.3**
		10*	$Al_{IV\text{-}Td}$	free	**-34.6**

* denotes the thermodynamically stable structure calculated at 800 K

Table S5. Aluminum sites on which μ_1-OH groups are bonded, nature of their H-bonds, and energy for the substitution of μ_1-OH sites by Cl on facets/edges of γ-Al_2O_3 crystallite dehydroxylated at 700 K if not specify otherwise. Entry marked by a * denotes the thermodynamically stable model calculated for a dehydroxylation at 800 K. Note: The first index after an Al atom indicates its coordination number and the second its VSEPR geometry (Oh: Octahedral, Td: Tetrahedral).

A) Chlorination of the basal $(110)_b$ facet model

On the basis of the stable structures of the basal $(110)_b$ facets, only the facet dehydroxylated at 700 K possesses suitable μ_1-OH to be substituted by Cl atoms. Indeed, the dehydroxylated facet with a facet coverage of 9.0 OH nm^{-2} exhibits a row of bridging HO-μ_2-(Al_{VI},Al_{VI}) and collinear OH-μ_1-Al_{IV} (**Figure S6**). While the bridging OH groups are free from H-bonds, terminal hydroxyls present at the facet are engaged in a linear hydrogen bonding network, where each hydroxyl is simultaneously H-donor and H-acceptor. Substitution of either of the non-equivalent μ_1-OH (site A, table S1) by Cl, leading to a Cl coverage of 1.1 Cl nm^{-2}, is an endothermic process by ca. +19 $kJ.mol^{-1}$. The positive enthalpy of exchange can be explained by the impact of the OH substitution by Cl on the hydrogen bond network. The short O-H···OH hydrogen bond (1.92 Å) is replaced by a longer O-H···Cl bond (2.14 Å). The breaking of this long range hydrogen bonding has for consequence an overall destabilization of the structure, making the chlorination process energetically disfavored on the $(110)_b$ facet. Such considerations related to the H-bond network disruption have been previously invoked in the literature.[3]

B) Chlorination of the lateral $(110)_l$ facet models

For the chlorination exchange study, the four different facet terminations, namely A1, A2, L1 and L2, were considered. Each substitution of OH by Cl on the $(110)_l$ model, leads to an increase of the Cl density by 1.5 Cl nm^{-2}. Firstly, the $(110)_l$-A1 model dehydroxylated at 700 K, with an OH coverage of 9.0 OH nm^{-2}, is the only one displaying terminal OH at its facet. Two possible sites are considered for the Cl exchange, the μ_1-OH (B), H-acceptor between the μ_2- and μ_3-OH facet sites and the HO-μ_1-Al_{IV} (C) that is involved in a HO-μ_2-(Al_{IV},Al_V) (**Figure S7**). While the

exchange of site C (-8.4 kJ.mol^{-1}) is slightly more exothermic than site B (-6.0 kJ.mol^{-1}), Cl substitution of both sites is energetically favored. Chlorine exchange at site (B) have a noticeable influence on μ_3-OH bond distance due to the removal of hydrogen bonding, leading to the shortening of the bond by 0.02 to 0.03 Å depending on the number of Cl exchanged.

In a second time, the $(110)_I$-A2 model at similar OH density (9.0 OH nm^{-2}) was considered for the Cl exchange. Analogous to the A1 termination, the A2 model is composed of two inequivalent terminal HO-μ_1-Al_{IV}, one exempt of any bridging HO in the direct coordination sphere of the Al ion (D), and one involved in a HO-μ_2-(Al_{IV},Al_{IV}) (F) (**Figure S8**). Substitution of the site (D) by Cl leads to a largely exothermic process (-30.8 kJ.mol^{-1}), slightly greater than the exchange observed for (E) (-24.3 kJ.mol^{-1}).

The two other terminations, namely L1 and L2 were considered with a OH density of 12 OH nm^{-2} (**Figure S9 and 10**), as it corresponds to the unique structures displaying terminal μ_1-OH in the range of pressure and temperature studied experimentally. In both cases, a single terminal OH is present, and its exchange by Cl leads to an exothermic reaction of -31.4 kJ.mol^{-1} for L1 (**Figure S9**, site F) and -23.4 kJ.mol^{-1} for L2 (**Figure S10**, site G).

C) Chlorination of the (111) facet models

Among all the (111) facets, only the D1 and D2 possess μ_1-OH, potential sites for the substitution by Cl. In all the cases under study, the exchange of terminal OH by Cl is either slightly (+5.7 kJ.mol^{-1}) or largely (+39.3 kJ.mol^{-1}) endothermic, making the chlorination of the (111) facet unlikely. The high endothermicity for the substitution of a terminal OH by Cl can be explained in two parts. Firstly, due to the large OH density (12.2 OH nm^{-2}), the terminal hydroxyls are in a hydrogen-bonding “nest”, disfavoring their substitution for a less stabilizing Cl atoms (**Figures**

S11, S12, S13). Secondly, the Al bearing the μ_1-OH is embedded in the sublayer, yielding a less accessible OH, subsequently more engaged in direct hydrogen-bonding with hydroxyls present at the upper layer of the (111) facet model.

D) Chlorination of the (100)/(110)$_l$-A1 edge model

This edge structure previously reported by Batista *et al.*[1] was identified as one of the preferential sites of exchange for Cl due to the presence of μ_1-OH groups free of hydrogen-bonding. The exchange energy for the chlorination of free μ_1-OH at the edge was previously discussed and correspond to -26.3 and -31.1 kJ.mol^{-1} for the edge model dehydroxylated at 700 K, and -38.4 kJ.mol^{-1} for the model dehydroxylated at 800 K (**Figures S14-S15**). It worth noticing that HO-μ_1-Al_{IV} (2) is not in direct coordination with μ_2-OH, leading to a more labile μ_1-OH and facilitating the Cl exchange reaction.

E) Chlorination of the (110)$_b$/(110)$_l$-L1 edge model

The DFT model for the edge between the (110)$_b$ and the (110)$_l$-L1 structure reveals 3 terminal hydroxyl sites present at the edge position for the thermodynamically stable model dehydroxylated at 700 K (**Figure S19**). Among the different possibilities, Cl exchange with the HO-μ_1-Al_{IV} site (10) leads to an exothermic reaction (-33.1 kJ.mol^{-1}) in the range of previously observed substitution on edge sites. Cl exchange with the terminal OH coordinated to Al_V (9) leads to a slightly less energetically favored reaction (-27.4 kJ.mol^{-1}). This decrease in exchange energy is even more pronounced for the substitution of the HO-μ_1-Al_{VI} site (8) with -15.5 kJ.mol^{-1}, corresponding to half the energy found for site (8). Substituting free μ_1-OH by Cl (9*) on the metastable model dehydroxylated at 800 K (**Figure S20**), corresponding to site (9) in the previous

dehydroxylation model, leads to a slight gain in energy (-35.3 kJ.mol^{-1}). Interestingly substitution of the μ_1-OH site (10*) present at the opposite edge is largely more exothermic than that of site (10) with an energy of -34.6 kJ.mol^{-1}. This case is similar to site (5*) observed for the $(110)_b$/$(110)_l$-A1, where the Al baring the μ1-OH undergoes a drastic reconstruction from an octahedral Al_V to a tetrahedral Al_{IV}.

SI 5. Calculated ^{1}H chemical shifts on the γ–alumina facets

The NMR (Nuclear Magnetic Resonance) chemical shifts were computed using the Gauge Including Projector Augmented Wave (GIPAW) method[4,5] on structures geometrically relaxed with a convergence criterion of 0.01 eV.Å^{-1}. The ^{1}H reference of chemical shift is the mean isotropic chemical shift calculated for the hydrogen atoms present in tetramethylsilane (TMS). The TMS molecule has been relaxed in a 20 Å cubic box at the gamma point. The energy cutoff for the plane waves was of 400 eV with the same smearing parameters as before, the same convergence criterion for the SCF cycles was used. The step size used for the finite difference k-space derivative in the linear response calculation was 0.003 Å^{-1}.

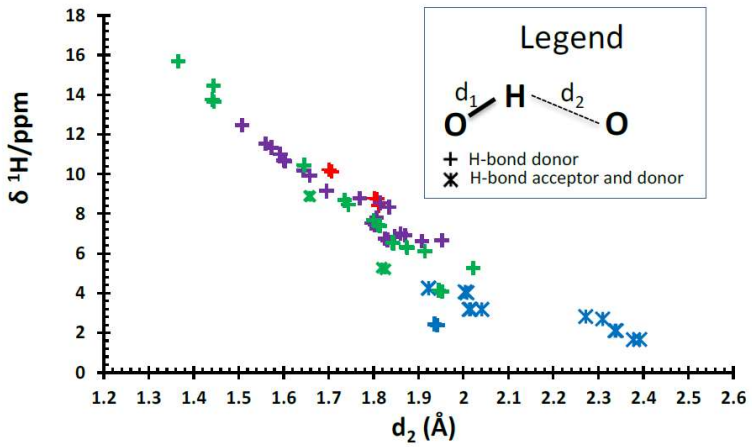

Figure S21. Evolution of the calculated chemical shift as a function of H-bond distance for H bond donor OH groups for the $(110)_{I}$-A1 facet and for all hydroxyls coverages. Blue symbols: μ_1-OH; green: μ_2-OH, red: μ_3-OH, purple μ_1-OH_2.

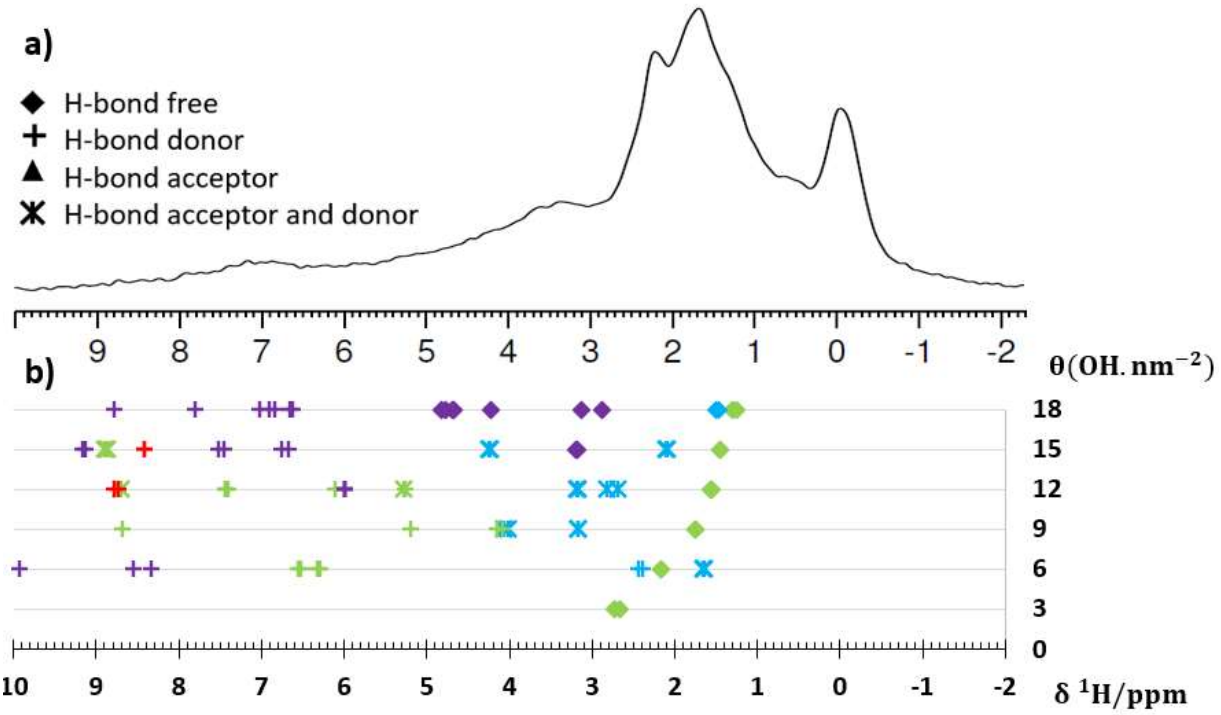

Figure S22. a) ^{1}H NMR spectrum of γ-alumina sample. **b)** Evolution of the calculated chemical shifts as a function of the water coverage. Case of the $(110)_{I}$-A1 facet. Blue: μ_1-OH, Green: μ_2-OH, Red: μ_3-OH, Purple: μ_1-H_2O.

T = 700 K; P_{H2O}= 10^{-4} bar; θ = 9.0 OH.nm^{-2}			T = 800 K; P_{H2O}= 10^{-6} bar; θ = 3.0 OH.nm^{-2}		
Specie	H-bond type	δ (ppm)	Specie	H-bond type	δ (ppm)
1 OH-μ_1-(Al_{IV})	Acceptor-donor	3.2	**1 OH-μ_2-(Al_{IV}-Al_{IV})**	**Free**	**2.7**
1 OH-μ_1-(Al_{IV})	Acceptor-donor	4.0 ; 4.1*	1 OH-μ_2-(Al_{IV}-Al_{IV})	Donor	14.5 ; 15.7*
1 OH-μ_2-(Al_{IV}-Al_{V})	Donor	10.4 ; 10.5*			
1 OH-μ_2-(Al_{V}-Al_{V})	**Free**	**1.7**			
1 OH-μ_2-(Al_{VI}-Al_{VI})	Donor	4.1			
1 OH-μ_3-(Al_{VI}-Al_{VI}-Al_{VI})	Donor	10.4 ; 10.5*			

Table S6. Calculated chemical shift for the $(110)_{I}$-A1 facet model for the relevant conditions of temperature and water pressure corresponding to NMR samples pretreatment. *The two values correspond to the protons belonging to symmetric OH groups (formally same specie) located on each side of the slab and which structures are not exactly the same.

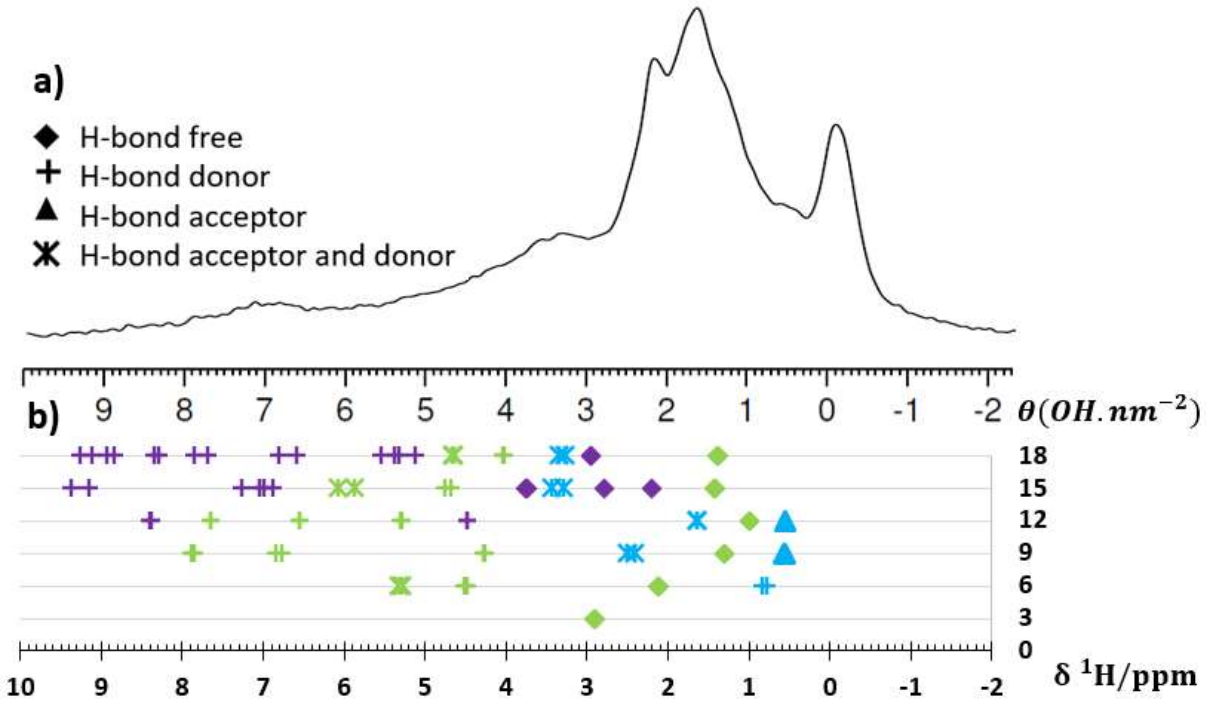

Figure S23. a) ^{1}H NMR spectrum of γ-alumina sample. **b)** Evolution of the calculated chemical shifts as a function of the water coverage. Case of the $(110)_{I}$-A2 facet. Blue: μ_1-OH, Green: μ_2-OH, Red: μ_3-OH, Purple: μ_1-H_2O.

T = 700 K; P_{H2O}= 10^{-4} bar; θ = 9.0 OH.nm^{-2}			T = 800 K; P_{H2O}= 10^{-6} bar; θ = 3.0 OH.nm^{-2}		
Specie	H-bond type	δ (ppm)	Specie	H-bond type	δ (ppm)
1 OH-μ_1-(Al_{IV})	Acceptor	0.5 ; 0.6	**1 OH-μ_2-(Al_{IV}-Al_{IV})**	**Free**	**2.9**
1 OH-μ_1-(Al_{IV})	Acceptor-donor	2.4 ; 2.5	1 OH-μ_2-(Al_{IV}-Al_{IV})	Donor	14.8 ; 14.9
1 OH-μ_2-(Al_V-Al_{VI})	Donor	6.8			
1 OH-μ_2-(Al_V-Al_V)	**Free**	**1.3**			
1 OH-μ_2-(Al_{VI}-Al_{VI})	Donor	4.3			
1 OH-μ_2-(Al_{IV}-Al_{IV})	Donor	7.8 ; 7.9			

Table S7. Calculated chemical shift for the $(110)_{I}$-A2 facet model for the relevant conditions of temperature and water pressure corresponding to NMR samples pretreatment. *The two values correspond to the protons of the symmetric OH groups located on each side of the nano-rod which structures are not exactly the same. *The two values correspond to the protons belonging to symmetric OH groups (formally same specie) located on each side of the slab and which structures are not exactly the same.

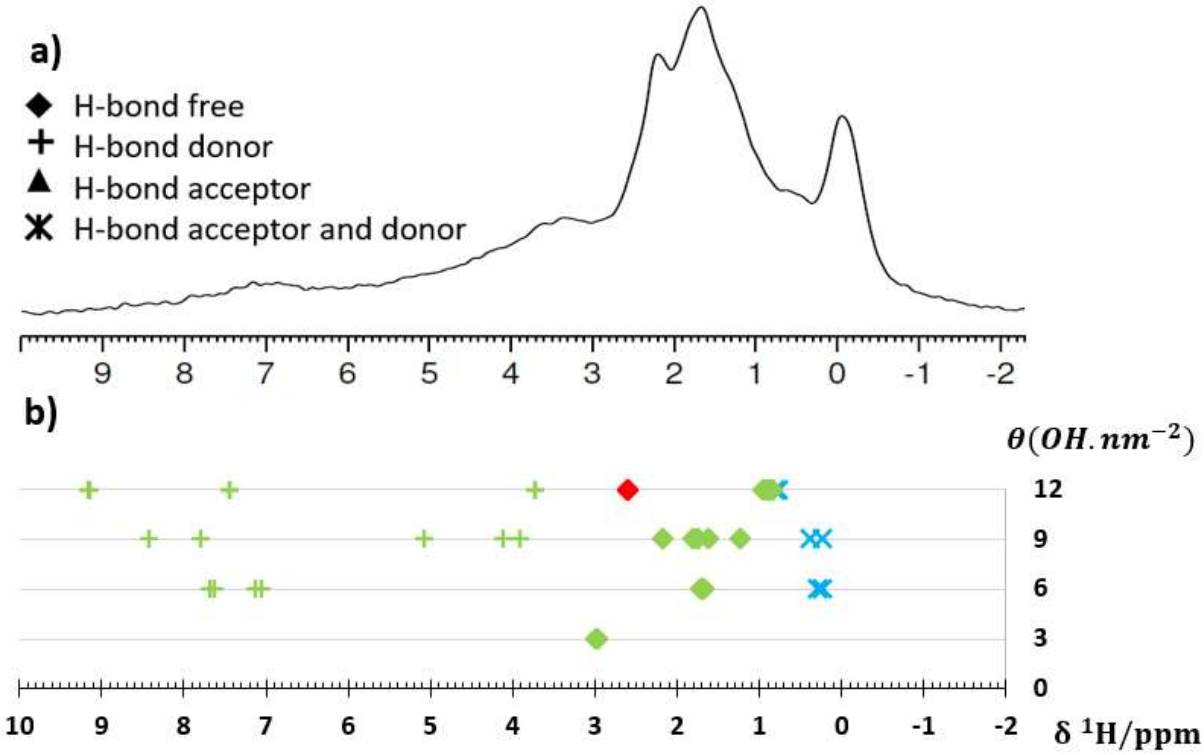

Figure S24. a) ^{1}H NMR spectrum of γ–alumina sample. **b)** Evolution of the calculated chemical shifts as a function of the water coverage. Case of the $(110)_{I}$-L1 facet. Blue: μ_1-OH, Green: μ_2-OH, Red: μ_3-OH.

T = 700 K; P_{H2O}= 10^{-4} bar; θ = 12.0 OH.nm^{-2}			T = 800 K; P_{H2O}= 10^{-6} bar; θ = 3.0 OH.nm^{-2}		
Specie	H-bond type	δ (ppm)	Specie	H-bond type	δ (ppm)
1 OH-μ_1-(Al_{IV})	Acceptor-donor	0.8	1 OH-μ_2-(Al_{IV}-Al_{IV})	Free	3.0
3 OH-μ_2-(Al_{VI}-Al_{VI})	Free	0.8 – 0.9	1 OH-μ_2-(Al_{IV}-Al_{IV})	Donor	14.2 ; 14.4*
1 OH-μ_3-(Al_{VI}-Al_{VI}-Al_{VI})	Free	2.6			
1 OH-μ_2-(Al_{IV}-Al_{VI})	Donor	9.2			
1 OH-μ_2-(Al_{VI}-Al_{VI})	Donor	4.3			
1 OH-μ_2-(Al_{VI}-Al_{VI})	Acceptor-donor	4.3			

Table S8. Calculated chemical shift for the $(110)_{I}$-L1 facet model for the relevant conditions of temperature and water pressure corresponding to NMR samples pretreatment. *The two values correspond to the protons belonging to symmetric OH groups (formally same specie) located on each side of the slab and which structures are not exactly the same.

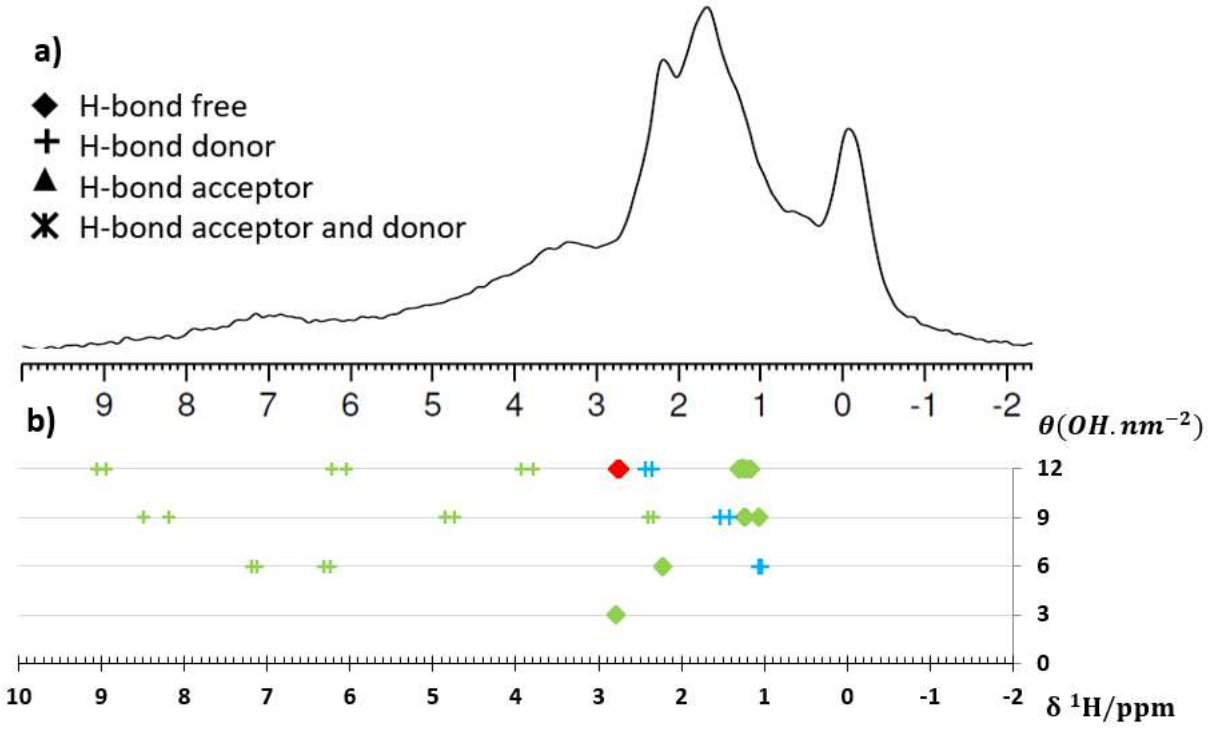

Figure S25. a) ^{1}H NMR spectrum of γ-alumina sample. **b)** Evolution of the calculated chemical shifts as a function of the water coverage. Case of the $(110)_{I}$-L2 facet. Blue: μ_1-OH, Green: μ_2-OH, Red: μ_3-OH.

T = 700 K; P_{H2O}= 10^{-4} bar; θ = 12.0 OH.nm^{-2}			T = 800 K; P_{H2O}= 10^{-6} bar; θ = 3.0 OH.nm^{-2}		
Specie	H-bond type	δ (ppm)	Specie	H-bond type	δ (ppm)
1 OH-μ_1-(Al_{IV})	Donor	2.3 ; 2.4*	1 OH-μ_2-(Al_{IV}-Al_{IV})	Free	3.0
3 OH-μ_2-(Al_{VI}-Al_{VI})	Free	1.2 – 1.3	1 OH-μ_2-(Al_{IV}-Al_{IV})	Donor	14.2 ; 14.4*
1 OH-μ_3-(Al_{VI}-Al_{VI}-Al_{VI})	Free	2.7 ; 2.8*			
3 OH-μ_2-(Al_{IV}-Al_{VI})	Donor	3.8 – 9.0			

Table S9. Calculated chemical shift for the $(110)_{I}$-L2 facet model for the relevant conditions of temperature and water pressure corresponding to NMR samples pretreatment. *The two values correspond to the protons belonging to symmetric OH groups (formally same specie) located on each side of the slab and which structures are not exactly the same.

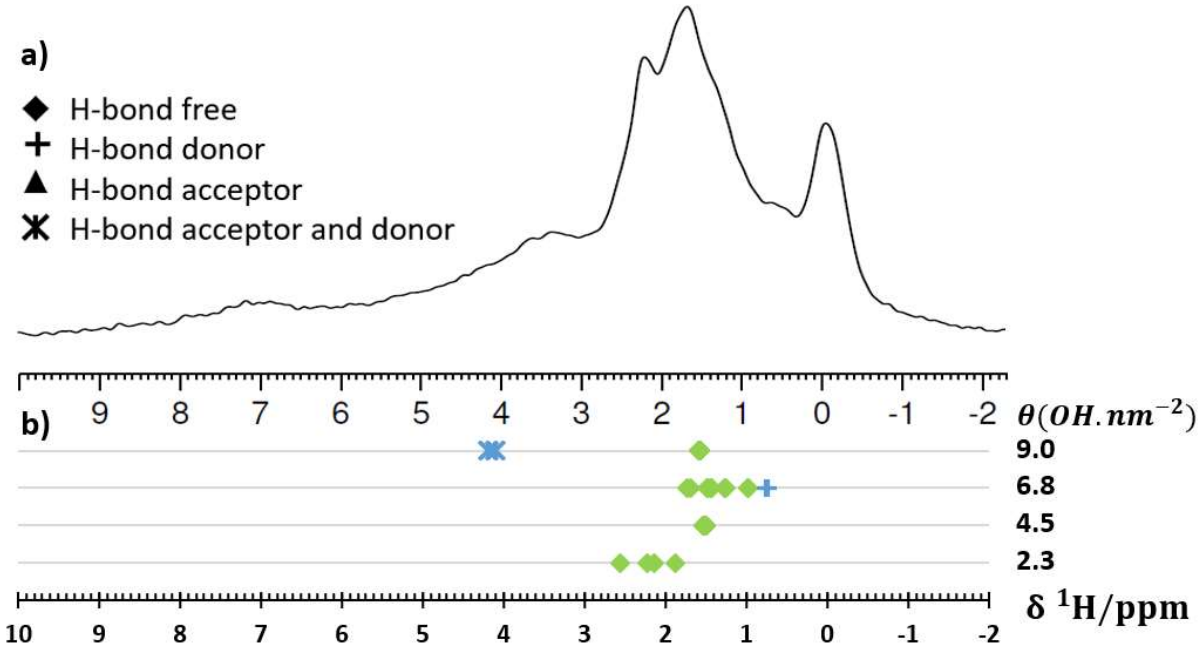

Figure S26. a) ^{1}H NMR spectrum of γ-alumina sample. **b)** Evolution of the calculated chemical shifts as a function of the water coverage. Case of the $(110)_b$ facet. Blue: μ_1-OH, Green: μ_2-OH.

T = 700 K; P_{H2O}= 10^{-4} bar; θ = 9.0 OH.nm^{-2}			T = 800 K; P_{H2O}= 10^{-6} bar; θ = 4.5 OH.nm^{-2}		
Specie	H-bond type	δ (ppm)	Specie	H-bond type	δ (ppm)
2 OH-μ_1-(Al_{IV}) 2 OH-μ_2-(Al_{VI}-Al_{VI})	Acceptor-Donor Free	4.1 – 4.2 1.6	2 OH-μ_2-(Al_{VI}-Al_{VI})	Free	1.5

Table S10. Calculated chemical shift for the $(110)_b$ facet model for the relevant conditions of temperature and water pressure corresponding to NMR samples pretreatment.

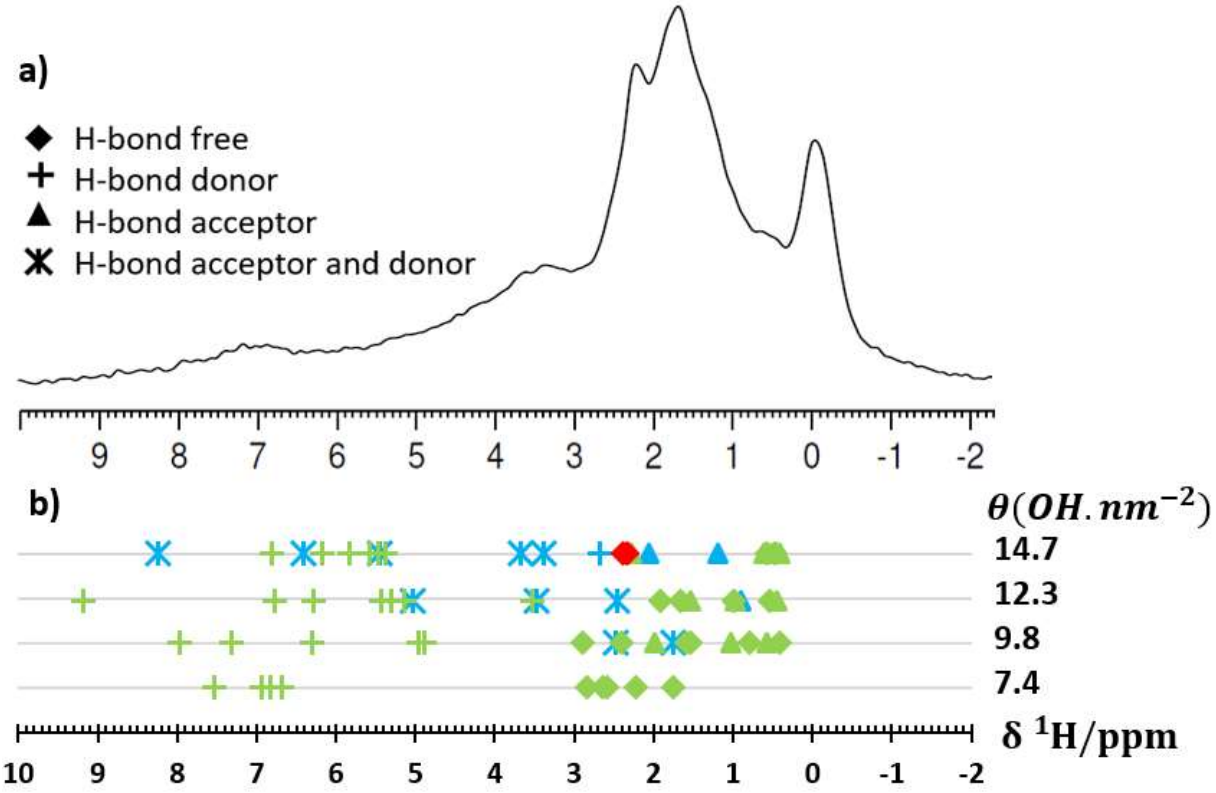

Figure S27. a) ^{1}H NMR spectrum of γ-alumina sample. **b)** Evolution of the calculated chemical shifts as a function of the water coverage. Case of the (111) D1 facet. Blue: μ_1-OH, Green: μ_2-OH, Red: μ_3-OH.

T = 700 K; P_{H2O}= 10^{-4} bar; θ = 9.8 OH.nm^{-2}			T = 800 K; P_{H2O}= 10^{-6} bar; θ = 9.8 OH.nm^{-2}		
Specie	H-bond type	δ (ppm)	Specie	H-bond type	δ (ppm)
1 OH-μ_1-(Al_{IV})	Acceptor-Donor	1.7 ; 2.5*	1 OH-μ_1-(Al_{IV})	Acceptor-Donor	1.7 ; 2.5*
1 OH-μ_2-(Al_{IV}-Al_{VI})	Acceptor	0.6 ; 1.0	1 OH-μ_2-(Al_{IV}-Al_{VI})	Acceptor	0.6 ; 1.0*
1 OH-μ_2-(Al_{IV}-Al_{VI})	Donor	8.0	1 OH-μ_2-(Al_{IV}-Al_{VI})	Donor	8.0
1 OH-μ_2-(Al_{V}-Al_{VI})	Donor	4.9 ; 6.3*	1 OH-μ_2-(Al_{V}-Al_{VI})	Donor	4.9 ; 7.3*
1 OH-μ_2-(Al_{VI}-Al_{VI})	Donor	5.0 ; 7.3*	1 OH-μ_2-(Al_{VI}-Al_{VI})	Donor	5.0 ; 7.3*
1 OH-μ_2-(Al_{IV}-Al_{VI})	Free	1.5 ; 1.6*	1 OH-μ_2-(Al_{IV}-Al_{VI})	Free	1.5 ; 1.6*
1 OH-μ_2-(Al_{V}-Al_{VI})	Free	2.4 ; 2.9*	1 OH-μ_2-(Al_{V}-Al_{VI})	Free	2.4 ; 2.9*
1 OH-μ_2-(Al_{VI}-Al_{VI})	Free	0.4 ; 0.8*	1 OH-μ_2-(Al_{VI}-Al_{VI})	Free	0.4 ; 0.8*

Table S11. Calculated chemical shift for the (111)-D1 facet model for the relevant conditions of temperature and water pressure corresponding to NMR samples pretreatment. *The two values correspond to the protons belonging to symmetric OH groups (formally same specie) located on each side of the slab and which structures are not exactly the same.

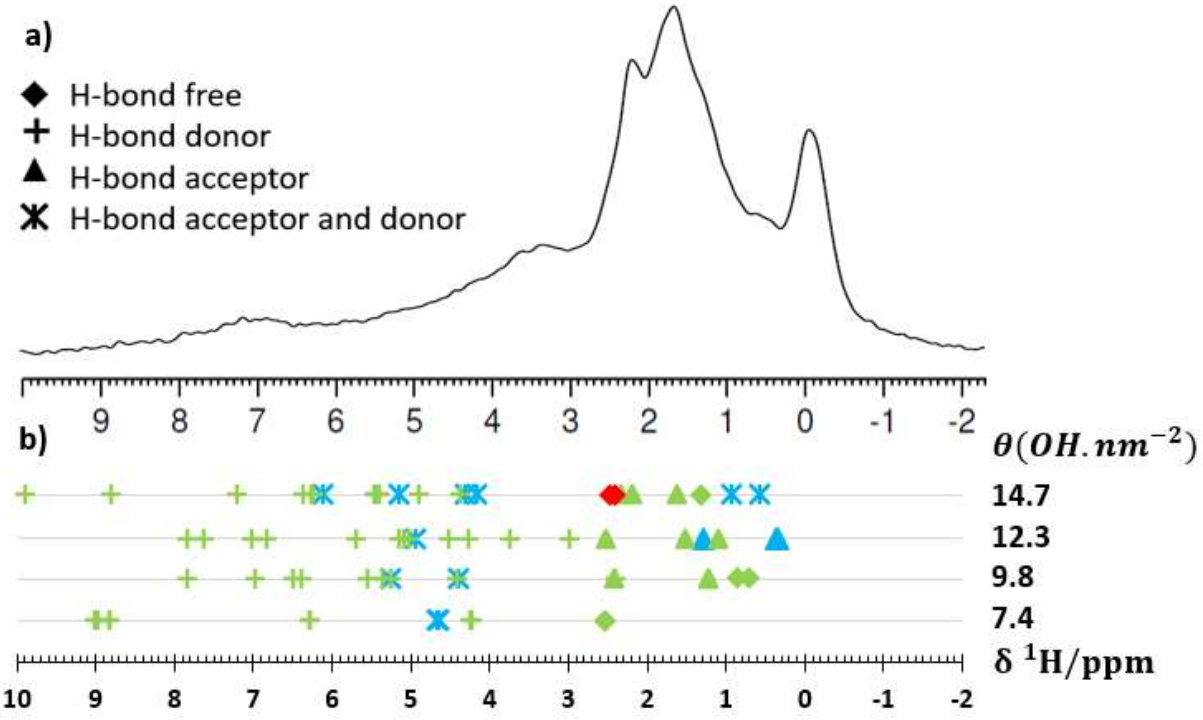

Figure S28. a) ^{1}H NMR spectrum of γ-alumina sample. b) Evolution of the calculated chemical shifts as a function of the water coverage. Case of the (111)-D2 facet. Blue: μ_1-OH, Green: μ_2-OH, Red: μ_3-OH.

T = 700 K; P_{H2O}= 10^{-4} bar; θ = 9.8 OH.nm^{-2}			T = 800 K; P_{H2O}= 10^{-6} bar; θ = 7.4 OH.nm^{-2}		
Specie	H-bond type	δ (ppm)	Specie	H-bond type	δ (ppm)
1 OH-μ_1-(Al_{IV})	Acceptor-Donor	4.4 ; 5.3*	1 OH-μ_1-(Al_{IV})	Acceptor-Donor	4.7
1 OH-μ_2-(Al_{VI}-Al_{VI})	Acceptor	1.2	1 OH-μ_2-(Al_{IV}-Al_{VI})	Free	2.5
1 OH-μ_2-(Al_{IV}-Al_{V})	Donor	5.5 ; 6.4*	4 OH-μ_2-(Al_{V}-Al_{VI})	Donor	4.2 – 9.0
1 OH-μ_2-(Al_{IV}-Al_{VI})	Donor	2.4 ; 6.4*			
3 OH-μ_2-(Al_{VI}-Al_{VI})	Donor	4.4 – 7.8			
1 OH-μ_2-(Al_{VI}-Al_{VI})	Free	0.7 ; 0.9*			

Table S12. Calculated chemical shift for the (111)-D2 facet model for the relevant conditions of temperature and water pressure corresponding to NMR samples pretreatment. *The two values correspond to the protons belonging to symmetric OH groups (formally same specie) located on each side of the slab and which structures are not exactly the same.

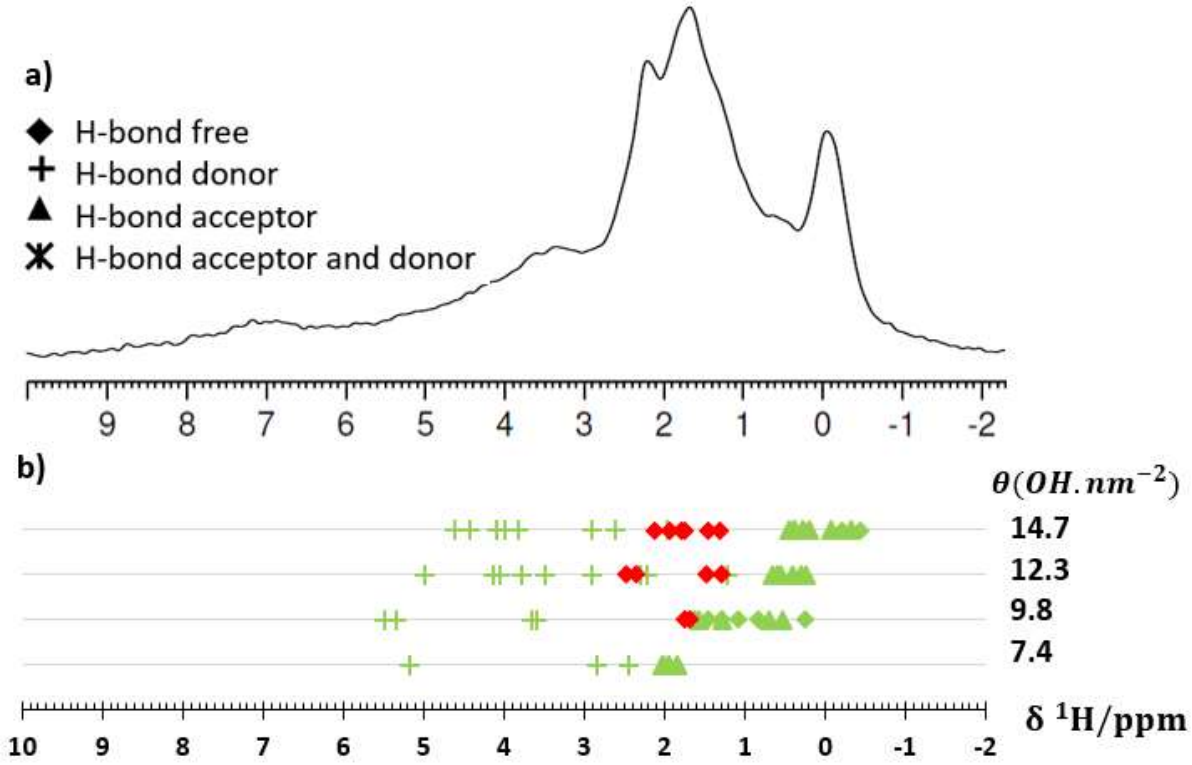

Figure S29. a) ^{1}H NMR spectrum of γ-alumina sample. **b)** Evolution of the calculated chemical shifts as a function of the water coverage. Case of the (111)-P1_2 facet. Blue: μ_1-OH, Green: μ_2-OH, Red: μ_3-OH.

T = 700 K; P_{H2O}= 10^{-4} bar; θ = 9.8 OH.nm^{-2}			T = 800 K; P_{H2O}= 10^{-6} bar; θ = 7.4 OH.nm^{-2}		
Specie	H-bond type	δ (ppm)	Specie	H-bond type	δ (ppm)
1 OH-μ_2-(Alv-AlvI)	Acceptor	1.3 ; 1.6*	1 OH-μ_2-(Alv-Alv)	Acceptor	1.8
1 OH-μ_2-(AlvI-AlvI)	Acceptor	0.5 ; 0.7*	2 OH-μ_2-(Alv-AlvI)	Acceptor	2.0
1 OH-μ_2-(Alv-AlvI)	Donor	5.3 ; 5.5*	1 OH-μ_2-(Alv-Alv)	Donor	2.8
1 OH-μ_2-(AlvI-AlvI)	Donor	3.6 ; 3.7*	2 OH-μ_2-(Alv-AlvI)	Donor	2.4 – 5.1
2 OH-μ_2-(Alv-AlvI)	Free	0.9 – 1.6			
1 OH-μ_2-(AlvI-AlvI)	Free	0.1 ; 1.2*			
1 OH-μ_3-(AlvI-AlvI-AlvI)	Free	1.7			

Table S13. Calculated chemical shift for the (111)-P1_2 facet model for the relevant conditions of temperature and water pressure corresponding to NMR samples pretreatment. *The two values correspond to the protons belonging to symmetric OH groups (formally same specie) located on each side of the slab and which structures are not exactly the same.

Structural model and T, P conditions	First hydroxyl group type | chemical shift	Second hydroxyl group | chemical shift	Approximate H-H distance
(111)-P1_2 800 K 10^{-6} bar	OH-μ_2-(Al_VAl_V) | 1.8	OH-μ_2-(Al_VAl_{VI}) | 2.0	4.7
	OH-μ_2-(Al_VAl_{VI}) | 2.0	OH-μ_2-(Al_VAl_{VI}) | 2.0	4.7
	OH-μ_2-(Al_VAl_V) | 1.8	OH-μ_2-(Al_VAl_{VI}) | 2.0	4.8
(111)-P1_2 700 K 10^{-4} bar	OH-μ_3-($Al_{VI}Al_{VI}Al_{VI}$) | 1.7	OH-μ_2-($Al_{VI}Al_{VI}$) | 0.5	2.7
	OH-μ_3-($Al_{VI}Al_{VI}Al_{VI}$) | 1.7	OH-μ_2-(Al_VAl_{VI}) | 1.3	2.7
	OH-μ_2-(Al_VAl_{VI}) | 1.3	OH-μ_2-($Al_{VI}Al_{VI}$) | 0.1	3.3
	OH-μ_2-($Al_{VI}Al_{VI}$) | 0.1	OH-μ_2-($Al_{VI}Al_{VI}$) | 0.5	2.8
	OH-μ_2-($Al_{VI}Al_{VI}$) | 0.1	OH-μ_2-(Al_VAl_{VI}) | 0.8	2.7
	OH-μ_2-(Al_VAl_{VI}) | 0.8	OH-μ_2-(Al_VAl_{VI}) | 1.0	3.6
	OH-μ_2-($Al_{VI}Al_{VI}$) | 0.1	OH-μ_2-(Al_VAl_{VI}) | 1.0	2.8
(111)-D1 700 K 10^{-4} bar 800 K 10^{-6} bar	OH-μ_2-($Al_{VI}Al_{VI}$) | 0.8	OH-μ_2-($Al_{VI}Al_{VI}$) | 1.0	2.8
	OH-μ_2-($Al_{IV}Al_{VI}$) | 1.5	OH-μ_2-($Al_{VI}Al_{VI}$) | 0.8	2.7
	OH-μ_2-($Al_{IV}Al_{VI}$) | 1.5	OH-μ_2-($Al_{VI}Al_{VI}$) | 1.0	2.9
	OH-μ_2-(Al_VAl_{VI}) | 2.5	OH-μ_2-($Al_{VI}Al_{VI}$) | 1.0	4.8
	OH-μ_2-($Al_{IV}Al_{VI}$) | 2.0	OH-μ_2-($Al_{VI}Al_{VI}$) | 0.4	2.7
	OH-μ_2-($Al_{IV}Al_{VI}$) | 2.0	OH-μ_2-($Al_{VI}Al_{VI}$) | 0.6	2.8
	OH-μ_2-($Al_{IV}Al_{VI}$) | 2.0	OH-μ_2-($Al_{IV}Al_{VI}$) | 1.6	2.9
(111)-D2 700 K 10^{-4} bar	OH-μ_2-($Al_{VI}Al_{VI}$) | 0.9	OH-μ_2-($Al_{VI}Al_{VI}$) | 1.2	2.6
	OH-μ_2-($Al_{VI}Al_{VI}$) | 0.9	OH-μ_2-($Al_{VI}Al_{VI}$) | 1.2	2.6
	OH-μ_2-($Al_{VI}Al_{VI}$) | 1.2	OH-μ_2-($Al_{VI}Al_{VI}$) | 1.2	2.7
	OH-μ_2-($Al_{VI}Al_{VI}$) | 0.9	OH-μ_2-($Al_{VI}Al_{VI}$) | 2.4	2.8
$(110)_I$-L1 700 K 10^{-4} bar	OH-μ_3-($Al_{VI}Al_{VI}Al_{VI}$) | 2.6	OH-μ_2-($Al_{VI}Al_{VI}$) | 0.9	2.8
	OH-μ_3-($Al_{VI}Al_{VI}Al_{VI}$) | 2.6	OH-μ_2-($Al_{VI}Al_{VI}$) | 0.9	2.8
	OH-μ_3-($Al_{VI}Al_{VI}Al_{VI}$) | 2.6	OH-μ_2-($Al_{VI}Al_{VI}$) | 0.9	4.8
	OH-μ_2-($Al_{VI}Al_{VI}$) | 0.9	OH-μ_2-($Al_{VI}Al_{VI}$) | 0.9	2.8
	OH-μ_2-($Al_{VI}Al_{VI}$) | 0.9	OH-μ_2-($Al_{VI}Al_{VI}$) | 0.9	2.8
	OH-μ_2-($Al_{VI}Al_{VI}$) | 0.9	OH-μ_2-($Al_{VI}Al_{VI}$) | 0.9	2.8
$(110)_I$-L2 700 K 10^{-4} bar	OH-μ_3-($Al_{VI}Al_{VI}Al_{VI}$) | 2.8	OH-μ_2-($Al_{VI}Al_{VI}$) | 1.2	2.8
	OH-μ_3-($Al_{VI}Al_{VI}Al_{VI}$) | 2.8	OH-μ_2-($Al_{VI}Al_{VI}$) | 1.2	2.8
	OH-μ_3-($Al_{VI}Al_{VI}Al_{VI}$) | 2.8	OH-μ_2-($Al_{VI}Al_{VI}$) | 1.3	4.8
	OH-μ_3-($Al_{VI}Al_{VI}Al_{VI}$) | 2.8	OH-μ_2-($Al_{VI}Al_{VI}$) | 1.2	2.8
	OH-μ_2-($Al_{VI}Al_{VI}$) | 1.2	OH-μ_2-($Al_{VI}Al_{VI}$) | 1.2	2.8
	OH-μ_2-($Al_{VI}Al_{VI}$) | 1.2	OH-μ_2-($Al_{VI}Al_{VI}$) | 1.3	2.8
	OH-μ_2-($Al_{VI}Al_{VI}$) | 1.2	OH-μ_2-($Al_{VI}Al_{VI}$) | 1.3	2.8
$(110)_b$ 700 K 10^{-4} bar	OH-μ_2-($Al_{VI}Al_{VI}$) | 1.6	OH-μ_2-($Al_{VI}Al_{VI}$) | 1.6	2.8
$(110)_b$ 800 K 10^{-6} bar	OH-μ_2-($Al_{VI}Al_{VI}$) | 1.5	OH-μ_2-($Al_{VI}Al_{VI}$) | 1.5	2.8

Table S14: Calculated chemical shifts (in ppm) of the protons located on two neighboring hydroxyl groups of non chlorinated alumina facets suspected to give rise to the observed ^{1}H-^{1}H correlations. The approximate H---H distance (in Å) deduced from the distances between O atoms bearing the protons of the corresponding hydroxyls is given in the last column (see main text for explanation).

SI 6. Hydration of edge models

The hydration of all edges was studied in three conditions: T = 800 K; $P_{H2O}=10^{-6}$ bar, (T = 700 K; $P_{H2O}=10^{-4}$ bar and T = 400 K; $P_{H2O}=10^{-2}$ bar. The last one does not correspond to any experimental condition but it is a complementary one which may be relevant from a more general point of view. The hydration states chosen for the facets are those reported in **Table S4**: these states were assumed to be kept fixed.

The free energies of water adsorption were computed assuming that the only temperature dependent value was the water free energy, through its translational and rotational enthalpy and entropy. For selected system, as analyzed in the previous study,[2] the vibrational components were neglected as they showed negligible effect on the computed surface dehydration temperatures. Therefore, the stability of the various structures is compared on the basis on the electronic energy calculated at 0 K. The water adsorption free energy $\Delta_{Ads}G$ ere computed according to equations (1). In some cases we also considered dehydration free energies which are computed by the same equations given $\Delta_{Adsorption}G = -\Delta_{dehydration}G$.

$$\Delta_{Ads}G\left(T, P_{H_2O}\right) = G_{Slab\ +\ n\ H_2O}(T) - G_{Slab\ +(n-1)\ H_2O}(T) - (1)\ G_{H_2O}\left(T, P_{H_2O}\right)$$
$$\approx E_{Slab+\ \ H_2O} - E_{Slab+(n-1)H_2O} - G^{*}_{H_2O}\left(T, P_{H_2O}\right) \quad (3)$$
$$G^{*}_{H_2O} = E_{elec}(H_2O) + G^{rot}_{H_2O}\left(T, P_{H_2O}\right) + G^{trans}_{H_2O}(T, P_{H_2O})$$

where n stand for the number of water molecules adsorbed. $\Delta_{Ads}G$ stands for successive hydration energies. The expressions of the rotational and translational free energies can be found in Ref.[6]

(100)/(110)$_l$-A1 edge

This case was described in detail in our previous work.[1] We simply recall the structures of the (110)$_b$/(110)$_l$-A1 edge at (T = 800 K; $P_{H2O}=10^{-6}$ bar) and (T = 700 K; $P_{H2O}=10^{-4}$ bar) in **Figures S14** and **S15**.

(110)$_b$/(110)$_l$-A1 edge

The structures of the (110)$_b$/(110)$_l$-A1 edge at (T = 800 K; $P_{H2O}=10^{-6}$ bar) and (T = 700 K; $P_{H2O}=10^{-4}$ bar) are illustrated in **Figures S17** and **S18**, while the energetics is reported in **Table S15**. The dehydration of the edge $Al_{IV\text{-}Td}$ was not considered. Indeed, such an edge hydroxyl has already been reported to be stable on the whole range of stability of γ–alumina.[2] The most dehydrated edge presented here presents two $Al_{IV\text{-}Td}$ linked to free edge μ_1-OH. The first two edge hydrations involve a dissociation of the water molecule on an Al site and lead to the formation of μ_1-OH. The remaining hydrogen is adsorbed on a nearby site, for the first hydration it is the edge O($Al_{(6)\text{-}IV}Al_{(5*)\text{-}V}$) and for the second one, it is an oxygen on the lateral surface. Beyond the first edge hydration, the hydroxyls become connected by H-bonds. The further hydration corresponds to non-dissociative water adsorptions.

The first hydration is the strongest, it is stable until 700 K and 10^{-4} bar of water pressure, at higher temperature and lower pressure, it becomes unstable. The subsequent hydrations have a slightly higher energy than those observed on (100) facet.[7,8] This similarity is due to the fact the in both cases, hydration of a Lewis acid site (Al_V) takes place. In practice, this edge will exhibit two Al_V Lewis acid sites, labelled as α and β in **Figures S17-S18**.

T = 800 K; $P_{H2O}=10^{-6}$ bar; $\theta_{(110)l\text{-}A1}$ = 3 OH.nm^{-2}; $\theta_{(110)b}$ = 4.5 OH.nm^{-2}	
Hydrated positions	$\Delta_{hydration}E(0K)$ | $\Delta_{hydration}G(800K, 10^{-6}$ bar)
0 H_2O	**None**
T = 700K; $P_{H2O}=10^{-4}$ bar; $\theta_{(110)l\text{-}A1}$ = 9 OH.nm^{-2}; $\theta_{(110)b}$ = 9 OH.nm^{-2}	
Hydrated positions	$\Delta_{hydration}E(0K)$ | $\Delta_{hydration}G(700K, 10^{-4}$ bar)
0 H_2O	None
1 H_2O: OH-$Al_{(5*)\text{-}V}$ / H-O($Al_{(6)\text{-}IV}Al_{(5)\text{-}V}$)	**-191 | -6**
2 H_2O: OH-$Al_{(5*)\text{-}V}$ / H-O($Al_{(6)\text{-}IV}Al_{(5)\text{-}V}$); OH-$Al_{\alpha\text{-}VI}$ / H-O($Al_{(7)\text{-}IV}$,Al_{IV})	-86 | 98
T = 400 K ; $P_{H2O}=10^{-2}$ bar ; $\theta_{(110)l\text{-}A1}$ = 15 OH.nm^{-2} ; $\theta_{(110)b}$ = 9 OH.nm^{-2}	
Hydrated positions	$\Delta_{hydration}E(0K)$ | $\Delta_{hydration}G(400K, 10^{-2}$ bar)
1 H_2O: : OH-$Al_{(5*)\text{-}V}$ / H-O($Al_{(6)\text{-}IV}Al_{(5)\text{-}V}$)	None
2 H_2O: OH-$Al_{(5*)\text{-}V}$ / H-O($Al_{(6)\text{-}IV}Al_{(5)\text{-}V}$); OH-$Al_{\alpha\text{-}VI}$ / H-O(Al_{VI},Al_{VI},Al_{VI})	-125 | -42
3 H_2O: OH-$Al_{(5*)\text{-}V}$ / H-O($Al_{(6)\text{-}IV}Al_{(5)\text{-}V}$); **$OH_2$-$Al_{\alpha\text{-}VI}$; OH-$Al_{\beta\text{-}VI}$ / H-O(Al_{VI},Al_{VI},Al_{VI})**	**-152 | -69**
4 H_2O: OH-$Al_{(5*)\text{-}V}$ / H-O($Al_{(6)\text{-}IV}Al_{(5*)\text{-}V}$); OH_2-$Al_{\alpha\text{-}VI}$; OH-$Al_{\beta\text{-}VI}$ / H-O(Al_{VI},Al_{VI},Al_{VI}); H_2O-$Al_{(5*)\text{-}VI}$;	-75 | 8

Table S15. Incremental hydration free energy (kJ mol^{-1}) of edge sites of the $(110)_b$/$(110)_l$-A1 edge model. The incremental hydration energy is computed between n+1 and n water molecule. For the last set of conditions (T = 400 K; $P_{H2O}=10^{-2}$ bar), a totally dehydrated edge was not considered as it would not be realistic considering the hydroxyl coverage of the facets. The notations of Al sites are those of **Figures S17 and S18**. The bold numbers correspond to the most stable structures at the given conditions.

$(110)_b/(110)_l$ -L1 edge

The same (T, P) conditions have been considered. The corresponding edge structures are illustrated in **Figures S19** and **S20** for two conditions relevant for NMR experiments, while the energetics is reported in **Table S16**. For similar reasons, as for the $(110)_b$/(110)l-A1 edge, the edge Al_{Td} dehydration was not considered. This last one should be hydrated on the whole range of gamma alumina stability. At higher temperature than 700 K and water pressure lower than 10^{-2} bar, it will remain free from H-bonds on edge 2. In those conditions, this Al_{IV} is neighboring two Lewis acid Al_V sites, which are labelled λ and γ in Figures S19-S20.

The first two hydrations occur on edge 1. The fourth hydration is more stabilizing than the third one because it allows the formation of two H-bonds. The same tendency as for the previous (110)/(110) edge arises: the hydrations energies are slightly higher than on the (100) facet.

T = 800 K; $P_{H2O}=10^{-6}$ bar; $\theta_{(110)l\text{-}L1}$ = 3 OH nm^{-2}; $\theta_{(110)b}$ = 4.5 OH nm^{-2}	
Hydrated positions	$\Delta_{hydration}E(0K)$ | $\Delta_{hydration}G(800K, 10^{-6}$ bar)
0 H_2O	**None**
T = 700 K; $P_{H2O}=10^{-4}$ bar; $\theta_{(110)l\text{-}L1}$ = 12 OH nm^{-2}; $\theta_{(110)b}$ = 9 OH nm^{-2}	
Hydrated positions	$\Delta_{hydration}E(0K)$ | $\Delta_{hydration}G(700K, 10^{-4}$ bar)
0 H_2O	**None**
1 H_2O: OH-$Al_{(9*)\text{-}V}$ / H-O(Al_{IV},$Al_{(9*)\text{-}V}$)	-172 | 13
2 H_2O: OH-$Al_{(9*)\text{-}VI}$ / H-O(Al_{IV},$Al_{(9*)\text{-}V}$); OH-$Al_{(9*)\text{-}VI}$ / H-O(Al_{VI},Al_{VI},Al_{VI})	-187 | -2
3 H_2O: OH-$Al_{(9*)\text{-}VI}$ / H-O(Al_{IV},$Al_{(9*)\text{-}V}$); OH-$Al_{(9*)\text{-}VI}$ / H-O(Al_{VI},Al_{VI},Al_{VI})	-149 | 35
OH-$Al_{\chi\text{-}VI}$ / H-O(Al_{VI},Al_{VI},Al_{VI})	
4 H_2O: OH-$Al_{(9*)\text{-}VI}$; OH-$Al_{(9*)\text{-}VI}$; OH-$Al_{\chi\text{-}VI}$; H_2O-$Al_{\gamma\text{-}VI}$	-166 | 19
5 H_2O: OH-$Al_{(9*)\text{-}VI}$; OH-$Al_{(9*)\text{-}VI}$; OH-$Al_{\chi\text{-}VI}$; H_2O-$Al_{\gamma\text{-}VI}$; H_2O-$Al_{\lambda\text{-}VI}$	-88 | 97
T = 400 K; $P_{H2O}=10^{-2}$ bar; $\theta_{(110)l\text{-}A1}$ = 15 OH nm^{-2}; $\theta_{(110)b}$ = 9 OH nm^{-2}	
Hydrated positions	$\Delta_{hydration}E(0K)$ | $\Delta_{hydration}G(400K, 10^{-2}$ bar)
0 H_2O	None
1 H_2O : OH-$Al_{(9*)\text{-}V}$ / H-O(Al_{IV},$Al_{(9*)\text{-}V}$)	-172 | -89
2 H_2O: OH-$Al_{(9*)\text{-}VI}$ / H-O(Al_{IV},$Al_{(9*)\text{-}V}$); OH-$Al_{(9*)\text{-}VI}$ / H-O(Al_{VI},Al_{VI},Al_{VI})	-187 | -104
3 H_2O : OH-$Al_{(9*)\text{-}VI}$ / H-O(Al_{IV},$Al_{(9*)\text{-}V}$); OH-$Al_{(9*)\text{-}VI}$ / H-O(Al_{VI},Al_{VI},Al_{VI})	-149 | -67
OH-$Al_{\chi\text{-}VI}$ / H-O(Al_{VI},Al_{VI},Al_{VI})	
4 H_2O : OH-$Al_{(9*)\text{-}VI}$; OH-$Al_{(9*)\text{-}VI}$; OH-$Al_{\chi\text{-}VI}$; H_2O-$Al_{\gamma\text{-}VI}$	-166 | -83
5 H_2O : OH-$Al_{(9*)\text{-}VI}$; OH-$Al_{(9*)\text{-}VI}$; OH-$Al_{\chi\text{-}VI}$; H_2O-$Al_{\gamma\text{-}VI}$; H_2O-$Al_{\lambda\text{-}VI}$	**-88 | -5**

Table S16. Incremental hydration free energy (kJ mol^{-1}) of different possible hydrations of the edge 1 and 2 of $(110)_b/(110)_l$-L1 edge with $\theta_{(110)l\text{-}L1}$ = 12 OH nm^{-2}; $\theta_{(110)b}$ = 9 OH nm^{-2}. The notations of Al sites are those of **Figures S19** and **S20**. The bold numbers correspond to the most stable structures at the given conditions.

$(110)_b$/(100) edge

As indicated in introduction of this section, to build this edge, we started from a γ–alumina nano-rod represented initially by the hypothetical $S_{0,0}$ matrix (as defined by Krokidis et al.[9]) for the bulk structure as it is not possible to obtain a stoichiometric rod by directly cleaving the $(110)_b$ slab model. The water molecules present are inherited from the boehmite (010) facet leading to the $(110)_b$ facet as explained in ref.2. Applying the Al migration scheme proposed by Krokidis et al.[9] in the bulk part of the nano-rod structure, a $S_{0,25}$ rod-like structure is obtained additional migration of Al atoms lead to the final structure of the hydrated rod.

The dehydration of the $(110)_b$ facet was done to consider the evolution of the edge site at high temperature and low water pressure. The only stable dehydration is on the facet nearby the edge 1. The μ_3-OH losses its proton together with the removal of one nearby μ_1-OH from the $(110)_b$ facet. This leaves one μ_1-OH on the $(110)_b$ facet which forms one μ_2-($Al_{IV}Al_{IV}$)-OH with the Al_{IV} on which was attached the other μ_1-OH which was removed. This edge model presented in **Figure S16** is the one stable in the range of conditions from 700 to 800 K and from 10^{-4} to 10^{-6} bar. This $(110)_b$/(100) edge model exhibits the same Al_{Td}-OH group at the edge position as the (100)/$(110)_l$-A1 edge proposed before.[1] The major difference is that the two edges of the $(110)_b$/(100) rod are composed only of Al_{Td} while on the (100)/$(110)_l$-A1 studied before, only one of the two edges presented these $Al_{IV\text{-}Td}$. For the same reasons as for the two previous nano-rods, these sites should remain hydrated on the whole range of gamma alumina stability. Other hydration or dehydrations would correspond to facet changes already studied in previous studies.[2,7,8]

SI 7. Calculated ^{1}H chemical shifts on the γ–alumina edges

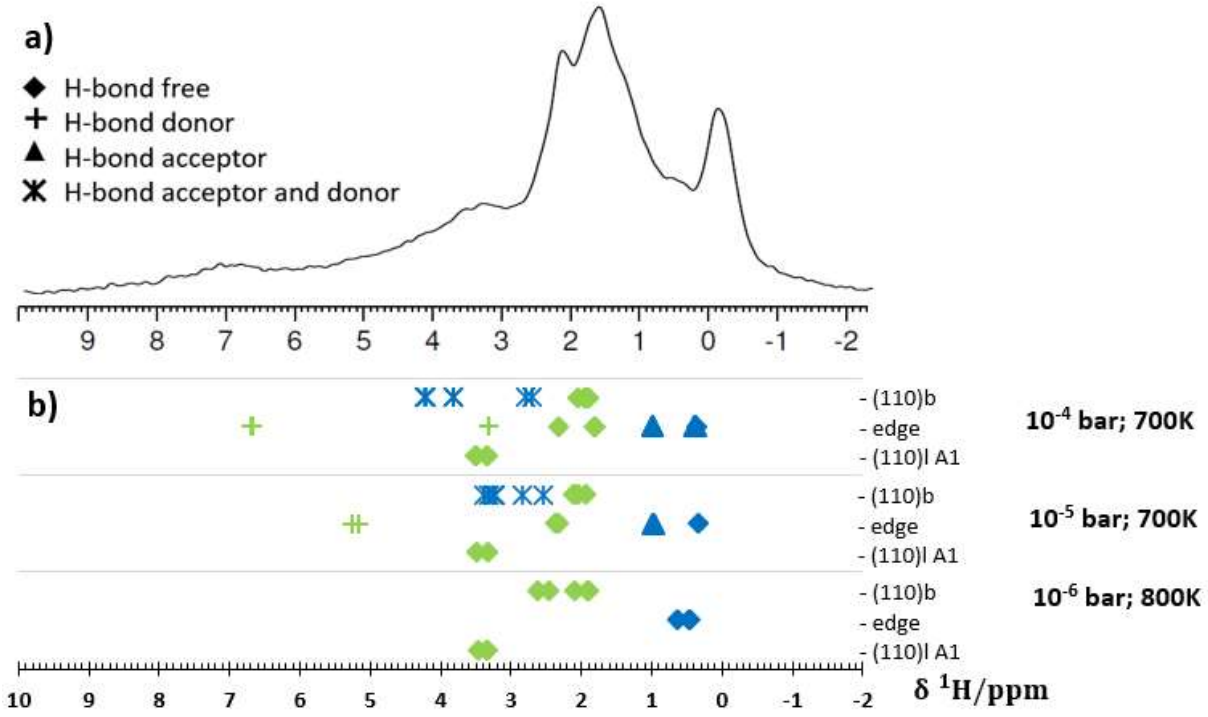

Figure S30: a) ^{1}H NMR spectrum of the γ-Al_2O_3 sample. **b)** Calculated chemical shifts on the $(110)_b/(110)_l$-A1 edge. Blue: μ_1-OH, Green: μ_2-OH, Red: μ_3-OH.

T = 700 K; P_{H2O}= 10^{-4} bar;			T = 800 K; P_{H2O}= 10^{-6} bar;		
Specie	H-bond type	δ (ppm)	Specie	H-bond type	δ (ppm)
1 OH-μ_1-(Al_{IV}) (7)	Free	0.4	2 OH-μ_1-(Al_{IV})	Free	0.5 – 0.6
1 OH-μ_2-(Al_{IV}-Al_V)	Donor	3.3			
1 OH-μ_1-(Al_V) (5)	Acceptor	0.4			
1 OH-μ_1-(Al_{IV}) (6)	Acceptor	1			
1 OH-μ_2-(Al_V-Al_{VI})	Donor	6.7			
2 OH-μ_2-(Al_V-Al_{VI})	Free	1.8 – 2.3			

Table S17: Calculated chemical shifts for the edge hydroxyls the $(110)_b/(110)_l$-A1 edge for the relevant conditions of temperatures and water pressures corresponding to NMR experiments.

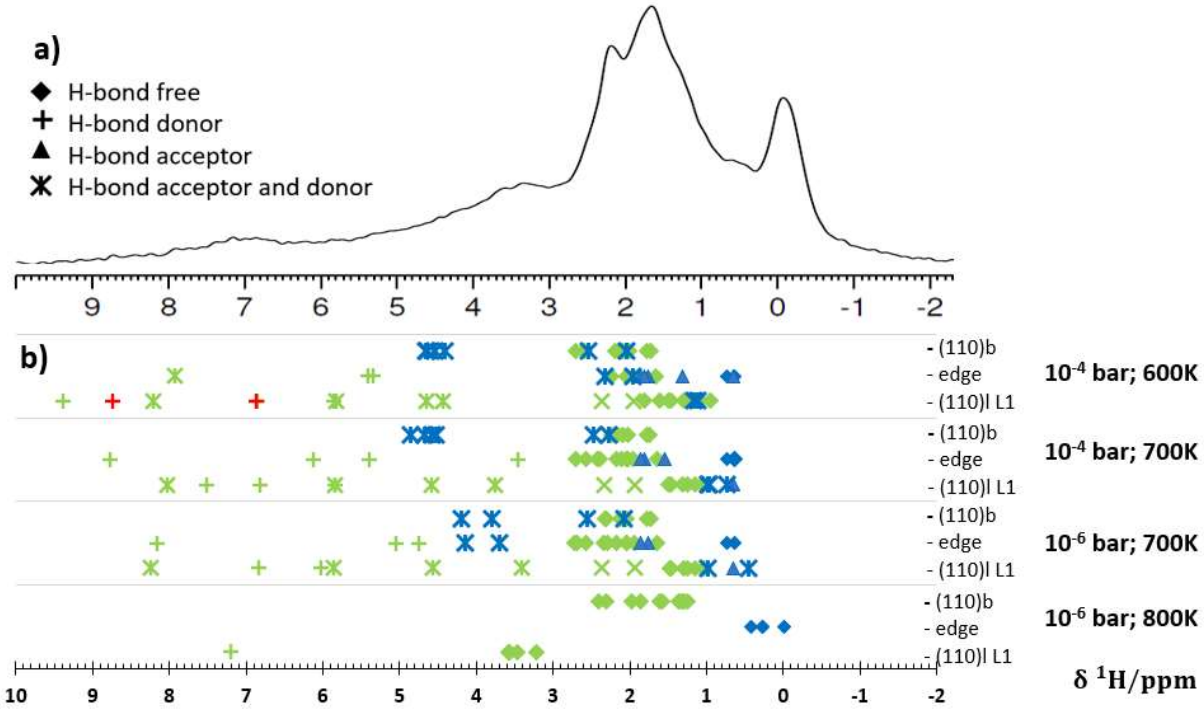

Figure S31: a) ^{1}H NMR spectrum of the γ-Al_2O_3 sample. **b)** Calculated chemical shifts on the $(110)_b/(110)_l$-L1 edge. Blue: μ_1-OH, green: μ_2-OH, red: μ_3-OH.

T = 700 K P_{H2O}= 10^{-4} bar			T = 800 K P_{H2O}= 10^{-6} bar		
Specie	H-bond type	δ (ppm)	Specie	H-bond type	δ (ppm)
1 OH-μ_1-(Al_{IV})	Free	0.6 - 0.7*	2 OH-μ_1-(Al_{IV})	Free	0.0 – 0.4
1 OH-μ_1-(Al_{IV})	Acceptor	1.8 - 1.9*			
1 OH-μ_2-(Al_{IV}-Al_V)	Donor	8.2 - 11.4*			
1 OH-μ_2-(Al_{IV}-Al_{VI})	Donor	4.7 - 5.0*			
1 OH-μ_2-(Al_{IV}-Al_{IV})	Free	2.6 - 2.7*			
1 OH-μ_2-(Al_{IV}-Al_{VI})	Free	2.3 - 2.7*			
1 OH-μ_2-(Al_V-Al_{VI})	Free	1.6 - 2.3*			

Table S18: Calculated chemical shifts for the edge hydroxyls the $(110)_b/(110)_l$-L1 edge for the relevant conditions of temperatures and water pressures corresponding to NMR experiments. *The two values correspond to the protons belonging to symmetric OH groups (formally same specie) located on each side of the nano-rod which structures are not exactly the same.

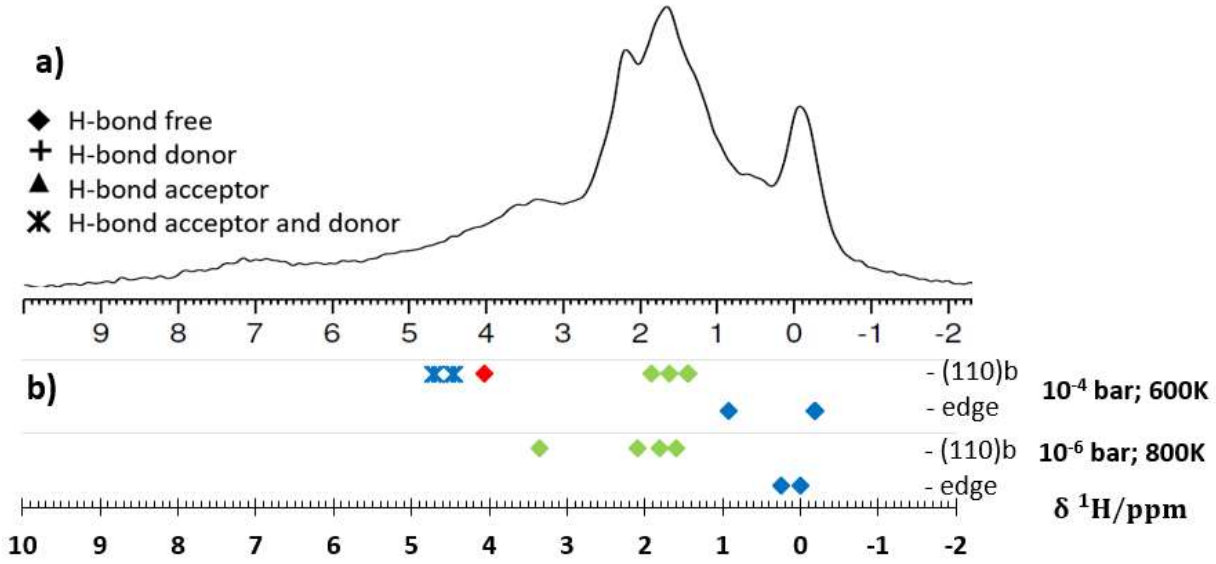

Figure S32: a) ^{1}H NMR spectrum of the γ-Al_2O_3 sample, **b)** Calculated chemical shifts on the $(110)_b$/(100) edge. Blue: μ_1-OH, green: μ_2-OH, red: μ_3-OH.

T = 700 K; P_{H2O}= 10^{-4} bar;			T = 800 K; P_{H2O}= 10^{-6} bar;		
Specie	H-bond type	δ (ppm)	Specie	H-bond type	δ (ppm)
2 OH-μ_1-(Al_{IV})	Free	0.0 – 0.3	2 OH-μ_1-(Al_{IV})	Free	0.0 – 0.3

Table S19: Calculated chemical shifts for the edge hydroxyls the $(110)_b$/(100) edge for the relevant conditions of temperature and water pressure corresponding to NMR samples pretreatment.

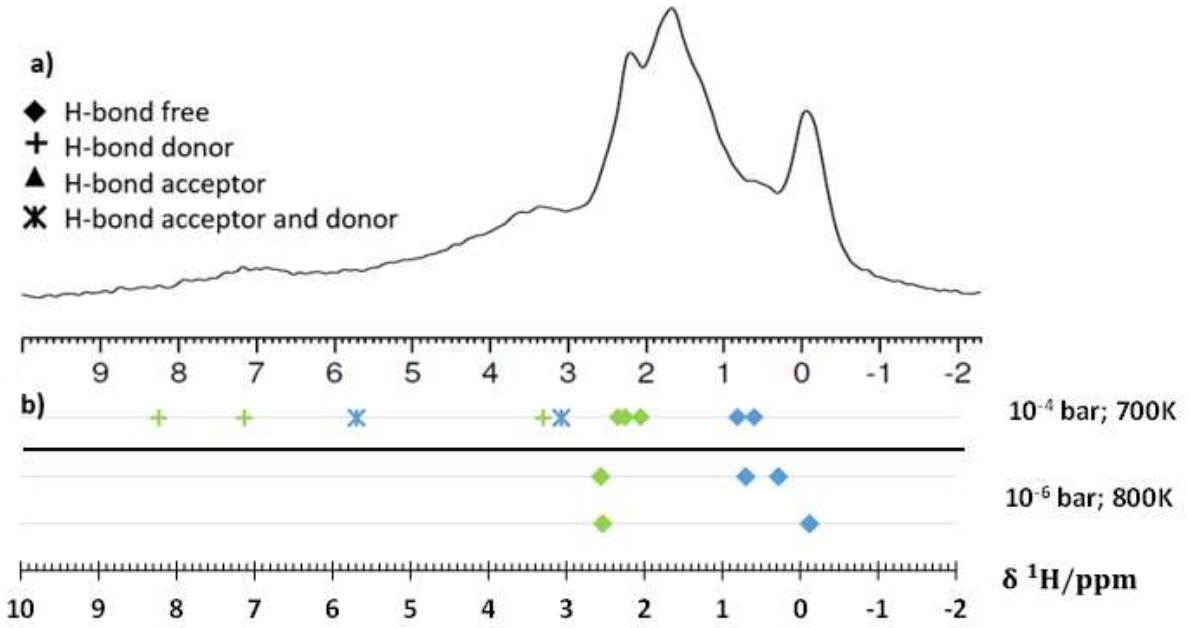

Figure S33: a) ^{1}H NMR spectrum of the γ-Al_2O_3 sample, **b)** Calculated chemical shifts on the (100)/(110)$_l$-A1 edge. Blue: μ_1-OH, green: μ_2-OH, red: μ_3-OH.

T = 700 K; P_{H2O}= 10^{-4} bar;			T = 800 K; P_{H2O}= 10^{-6} bar;		
Specie	H-bond type	δ (ppm)	Specie	H-bond type	δ (ppm)
2 OH-μ_1-(Al_{IV})	Free	0.6 – 0.9	1 OH-μ_1-(Al_{IV})	Free	-0.1
1 OH-μ_2-(Al_VAl_V)	Free	2.5	1 OH-μ_2-(Al_VAl_V)	Free	2.5

Table S20: Calculated chemical shifts for the edge hydroxyls the (100)/(110)$_l$-A1 edge for the relevant conditions of temperature and water pressure corresponding to NMR samples pretreatment.

Structural model and T, P conditions	First hydroxyl group type | chemical shift	Second hydroxyl group | chemical shift	Approximate H-H distance
$(110)_b/(100)$ 700 K 10^{-4} bar 800 K 10^{-6} bar	OH-μ_2-($Al_{VI}Al_{VI}$) | 1.8 OH-μ_2-($Al_{VI}Al_{VI}$) | 1.8 OH-μ_2-($Al_{VI}Al_{VI}$) | 1.6 OH-μ_2-($Al_{VI}Al_{VI}$) | 2.1 OH-μ_1-(Al_{IV}) | 0.0 OH-μ_1-(Al_{IV}) | 0.3	OH-μ_1-(Al_{IV}) | 0.3 OH-μ_2-($Al_{IV}Al_{IV}$) | 3.4 OH-μ_1-(Al_{IV}) | 0.0 OH-μ_1-(Al_{IV}) | 0.0 OH-μ_1-(Al_{IV}) | 0.0 OH-μ_1-(Al_{IV}) | 0.3	4.5 4.3 4.0 4.8 5.5 5.5
$(110)_b/(110)_t$-A1 800 K 10^{-6} bar	OH-μ_1-(Al_{IV}) | 0.6 OH-μ_1-(Al_{IV}) | 0.5 OH-μ_1-(Al_{IV}) | 0.5	OH-μ_2-($Al_{IV}Al_{VI}$) | 2.5 OH-μ_2-(Al_VAl_{VI}) | 2.6 OH-μ_2-($Al_{IV}Al_{IV}$) | 3.5	2.9 4.5 3.8
$(110)_b/(110)_t$-A1 700 K 10^{-4} bar	OH-μ_1-(Al_{IV}) | 0.4 OH-μ_1-(Al_{IV}) | 0.4	OH-μ_2-(Al_VAl_{VI}) | 2.3 OH-μ_2-($Al_{IV}Al_{IV}$) | 3.5	4.6 4.0
$(100)/(110)_t$-A1 700 K 10^{-4} bar	OH-μ_1-(Al_{IV}) | 0.9 OH-μ_1-(Al_{IV}) | 0.9	OH-μ_1-(Al_{IV}) | 0.6 OH-μ_2-(Al_VAl_V) | 2.5	4.2 4.1
$(110)_b/(110)_t$-L1 800 K 10^{-6} bar	OH-μ_1-(Al_{IV}) | 0.0 – 0.3 OH-μ_1-(Al_{IV}) | 0.3 – 0.4 OH-μ_1-(Al_{IV}) | 0.3 – 0.4	OH-μ_2-($Al_{IV}Al_{VI}$) | 2.0 OH-μ_2-(Al_VAl_{VI}) | 2.3 – 2.4 OH-μ_2-($Al_{IV}Al_{IV}$) | 3.5	2.9 4.4 4.2
$(110)_b/(110)_t$-L1 700 K 10^{-4} bar	OH-μ_1-(Al_{IV}) | 0.6 – 0.7 OH-μ_1-(Al_{IV}) | 0.6 – 0.7 OH-μ_1-(Al_{IV}) | 0.6 – 0.7	OH-μ_2-($Al_{IV}Al_{IV}$) | 2.6 – 2.7 OH-μ_2-(Al_VAl_{VI}) | 2.0 OH-μ_2-(Al_VAl_{VI}) | 1.6 – 1.9	2.8 4.7 5.0

Table S21: Calculated chemical shifts (in nm) of the protons located on two neighboring hydroxyl groups suspected to give raise to the observed ^1H-^1H correlations. The approximate H---H distance (in Å) deduced from the one of oxygen atoms of the corresponding hydroxyls is given in the last column. Bold values correspond to hydroxyl pairs which may correspond to cross-correlation observed by NMR (see main text).

model	Site Al_{IV}-Cl	Δδ (ppm)	model	Site Al_{IV}-Cl	Δδ (ppm)
$(110)_b$	A	4.6	$(100)/(110)_l$-A1	1	14.2
$(110)_l$-A1	B	7.5	$(100)/(110)_l$-A1	2	16.0
	C	7.1	$(100)/(110)_b$	3	13.1
$(110)_l$-A2	D	6.5	$(100)/(110)_b$	4	12.4
	E	7.8	$(110)_l$-A1/$(110)_b$	5	8.7
$(110)_l$-L1	F	6.7	$(110)_l$-A1/$(110)_b$	7	9.5
$(110)_l$-L2	G	6.0	$(110)_l$-L1/$(110)_b$	10	12.7
	Average facets	6.6		Average edges	12.4

Table S22. Calculated ^{27}Al chemical shift difference between Al_{IV}-μ_1-OH and Al_{IV}-Cl for facet and edge models for the relevant conditions of temperature and water pressure corresponding to the NMR experiments.

REFERENCES

(1) Batista, A. T. F.; Wisser, D.; Pigeon, T.; Gajan, D.; Diehl, F.; Rivallan, M.; Catita, L.; Gay, A. S.; Lesage, A.; Chizallet, C.; Raybaud, P.: Beyond γ–Al_2O_3 Crystallite Surfaces: The Hidden Features of Edges Revealed by Solid-State ^{1}H NMR and DFT Calculations. *J. Catal.* **2019**, *378*, 140-143.

(2) Pigeon, T.; Chizallet, C.; Raybaud, P.: Revisiting γ–Alumina Surface Models through the Topotactic Transformation of Boehmite Surfaces. *J. Catal.* **2022**, *405*, 140-151.

(3) Digne, M.; Raybaud, P.; Sautet, P.; Guillaume, D.; Toulhoat, H.: Atomic Scale Insights on Chlorinated Gamma-Alumina Surfaces. *J. Am. Chem. Soc.* **2008**, *130*, 11030-11039.

(4) Pickard, C. J.; Mauri, F.: All-Electron Magnetic Response with Pseudopotentials: NMR Chemical Shifts. *Phys. Rev. B: Condens. Matter* **2001**, *63,* 245101.

(5) Yates, J. R.; Pickard, C. J.; Mauri, F.: Calculation of NMR Chemical Shifts for Extended Systems Using Ultrasoft Pseudopotentials. *Phys. Rev. B* **2007**, *76,* 024401.

(6) *Computational Quantum Chemistry. Molecular Structure and Properties in Silico.*; McDouall, J. J. W., Ed.; Royal Society of Chemistry: Cambridge (UK), 2013.

(7) Digne, M.; Sautet, P.; Raybaud, P.; Euzen, P.; Toulhoat, H.: Hydroxyl Groups on Gamma-Alumina Surfaces: A DFT Study. *J. Catal.* **2002**, *211*, 1-5.

(8) Digne, M.; Sautet, P.; Raybaud, P.; Euzen, P.; Toulhoat, H.: Use of DFT to Achieve a Rational Understanding of Acid-Basic Properties of Gamma-Alumina Surfaces. *J. Catal.* **2004**, *226*, 54-68.

(9) Krokidis, X.; Raybaud, P.; Gobichon, A. E.; Rebours, B.; Euzen, P.; Toulhoat, H.: Theoretical Study of the Dehydration Process of Boehmite to Gamma-Alumina. *J. Phys. Chem. B* **2001**, *105*, 5121-5130.